# MASS TRANSFER IN SHEARED SUSPENSIONS OF NEUTRALLY BUOYANT PARTICLES: HYDRODYNAMIC DIFFUSION ACROSS A SUSPENSION AND INERTIAL EFFECTS ON INTERFACE MASS TRANSFER

A dissertation

Presented to the Faculty of the Graduate School

of Cornell University

in Partial Fulfillment of the Requirements for the Degree of

Doctor of Philosophy

by

Luying Wang

January 2008

# MASS TRANSFER IN SHEARED SUSPENSIONS OF NEUTRALLY BUOYANT PARTICLES: HYDRODYNAMIC DIFFUSION ACROSS A SUSPENSION AND INERTIAL EFFECTS ON INTERFACE MASS TRANSFER

Luying Wang, Ph.D.

Cornell University 2008

Mass transfer rate in dispersed multiphase flows can be increased dramatically by the random fluid velocity induced by the solid particles. In this study, the effects of solid particle volume fraction, the ratio of gap thickness of the Couette cell to the particle radius (H/a) and shear rate on the mass transfer rate are investigated in neutrally buoyant particle suspensions in simple shear flow. An electrochemical method is used to measure the mass transfer rate in the cylindrical Couette cell with solid particle volume fraction at 0.1, 0.17, 0.25, 0.33 and 0.4 with H/a=22 and 44. The experimental results show that the mass transfer rate increases with the shear rate, particle volume fraction and H/a. Lattice-Boltzmann/Fluid-tracer simulations are conducted with particle volume fraction at 0.1, 0.17 and 0.25 with H/a=10, 15 and 20. Tracer concentration profiles show that there is a bulk region and boundary layers. In the bulk region, hydrodynamic diffusion is dominant and in the boundary layers, molecular diffusion is important. A simple two-parameter model with the parameters determined from simulations yields predictions that are in good agreement with the experiments.

Mass transfer from neutrally buoyant freely rotating spheres to the bulk in simple shear flow with inertial effect is studied experimentally. Ion exchange beads are used for the mass transfer study. The radius of the ion exchange particle is 275μm which makes the Re up to 1.5 and Pe up to 15,000. The experimental results agree well with the recent theoretical work.

# BIOGRAPHICAL SKETCH

Luying Wang was born on November 27, 1973 and raised in Heilongjiang Province, located in northeast of China. She spent seven years in Beijing and earned her bachelor degree from Beijing University of Chemical and Technology in 1996 and Master degree from Chinese Academy of Sciences in 1999, both in Chemical Engineering. In 1999, she decided to go abroad for her Ph.D. study and accepted the admission offer from University of Connecticut. The study at University of Connecticut ended up with another Master degree in Chemical Engineering. In 2002 spring, she joined Prof. Donald Koch's group at Cornell University to continue her Ph.D. study on multiphase flow.

ACKOWLEDGMENTS

I would like to thank my advisor and committee chairman Prof. Donald Koch. His extraordinary intelligence and knowledge have guided me throughout all my Ph.D. study. I would also like to thank my other two committee members, Prof. Claude Cohen and Prof. Michel Louge. I thank Prof. Cohen for sitting in our group meetings and providing with thoughtful ideas for my experiments. I thank Prof. Louge for his time being my committee member and giving helpful suggestions for my thesis.

I also want to thank all my colleagues in Prof. Koch's group. They provided me with a friendly and encouraging environment for my study.

Finally, I would thank my husband, Hongliang Sun, and my daughter Lucy Sun. Without their love and support, I could not finish this long journey.

TABLE OF CONTENTS

LIST OF TABLES

LIST OF FIGURES

# Chapter 1. Introduction

The mass and heat transport mechanisms in a flowing suspension are different from those in a stationary fluid because of the random motion of particles. The convection associated with the randomly fluctuating velocity in the continuous phase induced by the dispersed particles is an important factor influencing the heat and mass transport in these applications. The rate of particle-induced transport can be much larger than the rate of Brownian diffusion, which is the only mechanism of mass transport in a stationary fluid. Therefore, the effective diffusivity for transport normal to the bulk flow in a sheared suspension can be much larger than that in the stationary suspension.

Heat and mass transport in the bulk of a suspension is controlled by hydrodynamic diffusion. The hydrodynamic diffusion is caused by the random fluid velocity induced by the solid particles. Because of the no-slip boundary conditions, the hydrodynamic diffusivity goes to zero near the walls and molecular diffusion becomes relatively important in a thin boundary layer near the walls, as shown in Figure 1.1. The concentration gradient in the bulk region is small and a constant and concentration gradient is steep in the boundary layers.

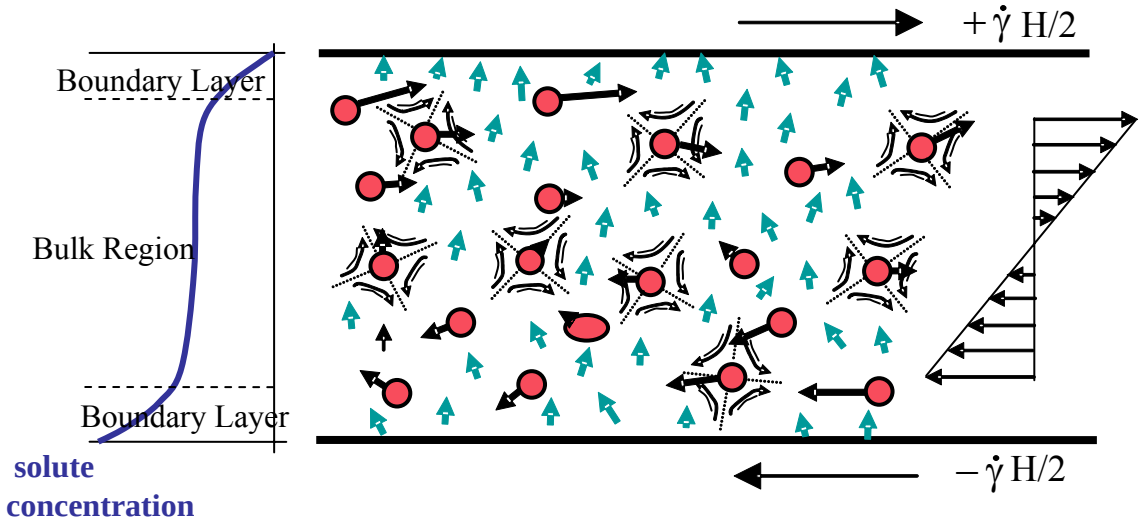


Figure 1.1. Mass transport process in sheared neutrally buoyant particle suspension. Larger spheres represent the solid particle neutrally buoyant in the fluid. The arrows represent the tracers transported from the lower wall to the upper wall.

For infinitely dilute suspensions in which particle-particle interaction can be neglected, theoretical results for mass enhancement have been presented by Leal (1973) for low Pe, and Nir and Acrivos (1976) for high Pe, where Pe is defined as

$$Pe = \frac{\dot{\gamma} a^2}{D}$$

Where $\dot{\gamma}$ is the shear rate;

a is the radius of the solid particle;

D is the molecular diffusivity;

At $\Phi \to 0$, Leal predicts that mass enhancement is proportional to $Pe^{3/2}$ for $Pe \to 0$ and $Pe^{1/11}$ by Nir and Acrivos for $Pe \to \infty$. However, $\Phi$ =0.1 to 0.4 are much too concentrated for particle-particle interaction to be neglected.

Koch (1996) obtains a scaling analysis for the heat and mass transport in a sheared neutrally buoyant particle suspension. Heat and mass transport in the bulk of a suspension is controlled by hydrodynamic diffusion at high Peclet number. The hydrodynamic diffusion is caused by the random motion of particles. The hydrodynamic diffusivity far from the walls is given by $D^* = d_2 \dot{\gamma} a^2$, where $d_2$ is a dimensionless function of volume fraction and is proportional to $\Phi^2$. However, the no-slip boundary condition requires the fluid velocity goes to zero quadratically as approaches the walls. By scaling analysis, the hydrodynamic diffusivity near the wall is $D^* = d_3 \dot{\gamma} y^4 / a^2$, where $d_3$ is a dimensionless function of $\Phi^2$ at small volume fractions. Thus, molecular diffusion becomes relatively important in a thin boundary layer near the walls. Then by evaluating concentration gradient within boundary layers and in the bulk of suspension, combining with the definition of the Nusselt number and Peclet number, the final relationship between Nu and Pe is shown as follows.

$$\frac{1}{Nu} = \frac{1}{d_2 Pe} + \frac{\pi a}{2^{1/2} H (d_3 Pe)^{1/4}}$$

Where Nu is defined as $Nu = \frac{hH}{D}$

H is the gap thickness;

h--mass transfer coefficient;

$d_2$ and $d_3$--coefficients determined from experimental data

Wang and Keller (1978, 1985) measure the diffusion of ions in a Couette cell with blood cell suspensions. The gap of the Couette cell, H, is 460 μm and the radius of red blood cell, a, is 4.2 μm, so the ratio of gap thickness to the particle radius, H/a, is 110. Peclet number ranges from 5 to 100. Volume fraction varies from 0.18 to 0.45. It is found that shearing the suspension gives rise to an enhancement of the transport that is almost linear with shear rate.

Sohn and Chen (1981) measure the heat transfer in a Couette cell with polyethylene particles and polystyrene particles neutrally buoyant in the mixture of silicone oil and kerosene. The ratio of gap thickness to the particle radius is 18 for polyethylene and H/a is 160 for polystyrene particles. Peclet number varies from 0 to 500. And volume fractions change from 0.15 to 0.3. The augmentation of the heat transfer caused by the shear for H/a=18 is significantly less than the augmentation of the mass transfer in Wang and Keller's experiment. Sohn and Chen also observe that the augmentation of the heat transfer due to shear is much larger with a suspension of smaller polystyrene spheres for which H/a=160 than for the large polyethylene spheres. However, the data for the small spheres is limited to Pe < 10.

The discrepancy between Wang & Keller's and Sohn & Chen's experimental data can be explained by the Koch theory. The mass transfer experiments with a large gap to particle diameter ratio, eg. H/a=110 in Wang and Keller's experiments, exhibiting a nearly linear increase of the Nusselt number with Peclet number can be due to hydrodynamic diffusion. The much slower increase in the heat transfer rate at a

smaller gap to particle radius ratio, eg. H/a=18 in Sohn and Chen's experiments, can be attributed to the importance of the boundary layer resistance.

But the previous experimental study does not provide enough data to test the Koch theory. It would be desirable to have a single experiment that spans a range of values of H/a, volume fraction, Peclet number and Reynolds number. Also, in the Koch theory, $d_2$ and $d_3$ need to be determined before it can be used for prediction. Therefore, simulations are included in this study. The advantage of the simulation over experiments is that by tracer method, the detailed concentration profile can be obtained. So the resistance of bulk region and boundary layer can be studied separately. Also, it is convenient to vary Peclet number and Reynolds number and study these two effects independently.

We use an electrochemical technique to measure the rate of mass transport across the gap of cylindrical Couette cell containing a suspension. The Couette cylinders are partly coated with nickel and act as the anode and cathode of an electrolytic cell. The mass flux is determined from the current flowing from anode to cathode. The current is carried by a pair of ions, ferricyanide and ferrocyanide, that undergo oxidation and reduction reactions at the electrode surface. The suspending fluid also contains an excess of an electrolyte that does not react at the nickel surface. This electrolyte forms electrical double layers at the electrode surfaces that screen the electric field. As a result, the flux of the redox ions across the gap is controlled by convection and diffusion and not by migration due to an electric field. The redox ion pair and nickel electrode surface are chosen because they have a fast reaction rate. As long as the reaction rate is fast compared with the rate of mass transport, the reaction reaches a local equilibrium. An analysis of this local equilibrium condition shows that the current reaches a constant limiting value for large enough electrical potential

difference between cathode and anode. This limiting current gives a measurement of the mass transfer coefficient.

The velocity disturbances in the suspensions can be caused by the shearing of the fluid and/or by the buoyancy driven flow of the particles relative to the fluid. To understand the phenomenon clearly, it is useful to isolate the effect of shear by considering the case of neutrally buoyant particles. Therefore, we study transport in a neutrally buoyant particle suspension subject to shear flow in a cylindrical Couette cell.

We emphasize large Peclet numbers where the heat and mass transport is dominated by convection except in thin boundary layers near walls of the Couette. In the experiments, polystyrene particles with range of radii of about 100-250 μm are used. With shear rates of 0-120/second in aqueous solutions this generates particle Reynolds numbers up to 6.6 and Peclet numbers up to 15,870. The gap thickness is 5 mm which makes the H/a changing from 22 to 44. This is a range in which we can expect to see a competition between bulk and boundary layer resistances to mass transfer.

The experiments will be performed primarily for particle volume fractions of about 0.1 to 0.4. Experimental measurements of the hydrodynamic diffusion of solid particles at low Reynolds numbers indicate that the effects are most significant for volume fractions larger than about 0.2. We expect that the enhancement of mass transport of tracer particles over a range of Reynolds numbers addressed in the present study may also be more pronounced for volume fractions above 0.2.

We also perform numerical simulations of the mass transport in neutrally buoyant particle suspensions. The simulation geometry consists of a suspension of spherical particles confined between two planar walls. Periodic boundary conditions are applied in the two directions perpendicular to the walls. We use a tracer method to simulate the transport of ions in the flow field. It has been shown that the convection-

diffusion process of passive species (solute, ions, etc.) in a flow field can be modeled by the motion of tracers governed by the Langevin equation (Brenner and Edwards, 1993). These tracers undergo Brownian diffusion as well as being convected by the fluid velocity field computed by the lattice-Boltzmann method. This tracer method is able to give the time averaged flux and concentration profiles as functions of y. This tracer method is particularly useful for moderate-to-high Peclet number flows because it does not require a refined computational grid to resolve the diffusion boundary layers. It has been used by many authors to study dispersion problems in fixed beds [Manz et al. 1999; Reynolds et al. 2000; Reynolds 2002; Yashino and Inamuro 2002; Maier et al. 2003; Freud et al. 2005; Bijeljic and Blunt 2006]. To our knowledge, it has not been applied to dynamic simulations where the positions of particles and the velocity field are constantly evolving.

The simulations can provide time averaged profiles of velocity and tracer concentration. We then can differentiate the boundary layer and bulk resistances to evaluate $d_2$ and $d_3$ in the Koch theory.

In the chapter 2, section 1 focuses on the experimental study, section 2 discusses the simulations and section 3 is the comparison of the experimental results and simulation results to the theoretical prediction.

In the chapter 3, experiments of mass transfer from a neutrally buoyant particle to the fluid are discussed.

It has been known since the work of Acrivos (1971) that, in the absence of inertia (Re=0), the heat transfer and mass transfer from neutrally buoyant freely rotating spheres in simple shear flow is diffusion limited at large Peclet number.

This results from the presence of closed streamlines which completely surrounds the rotating sphere. As a result, fluid elements near the sphere move around it in periodic orbits, being unable to carry heat or mass away. Acrivos (1971) shows

that Nu approaches 9, i.e. 4.5 times its value of pure conduction or diffusion, for Pe $\rightarrow$ $\infty$ when Re=0, where Nu is defined as $Nu = 2ha/D$, h is the mass transfer coefficient.

Inertial effects become important in suspensions of large particles or in relative low viscosity fluid. In sheared suspensions, microscale inertia is characterized by the particle Reynolds number, a dimensionless ratio of the magnitudes of inertial and viscous forces on the scale of a single particle.

When Re is small but nonzero, Subramanian and Koch (2006) showed that centrifugal forces break the closed-streamline that allows heat or mass to be convected away in an efficient way. It is then found that the dimensionless heat and mass transfer rate or Nusselt number is given by

$$Nu = (0.65 - 0.0828\,\mathrm{Re}^{\frac{1}{2}})(\mathrm{Re}\,Pe)^{\frac{1}{3}} + O(1) \quad \text{for Re<<1 and PeRe>>1.}$$

But to our knowledge, there is no experimental data reported for this problem.

We use the ion exchanger to study the mass transfer from the single particle to the fluid. Ion exchanger has been used by many people for mass transfer study (Calderbank, 1961, Harriott, 1962, Kuboi, 1974, Yagi, 1984, Asai, 1988, Armenante, 1994). The radius of the ion exchanger particle is 275μm which makes the Re up to 1.5 and Pe up to 15,000. We also compare our experimental results with the simulations by Yang et al. (2007).

# Chapter 2. Hydrodynamic Diffusion across a Suspension

## 1. Experiment, Results and Discussion

### 1.1 Experiment

The measurement of the mass transfer rate in sheared neutrally buoyant particle suspensions can be obtained using an electrochemical technique to measure the rate of mass transport between the two cylinders of a Couette cell for a certain imposed ion concentration difference. Two different types of monodispersed polystyrene particles were used in the experiments: radii were 115μm and 230μm respectively. The shear rate was varied from 0 to 150/second to explore the effects of the Peclet numbers, Reynolds numbers and the ratio of the gap thickness to the particle radius (H/a) on the transport rate. The Reynolds number was varied up to a value of 6.6 and Peclet numbers up to 15,870 were achieved. The gap thickness of the Couette cell was 5 mm. The volume fraction of the polystyrene particles was varied from 0.1 to 0.4.

#### 1.1.1 Principle of the electrochemical method

To establish the principle of the method, the suspension was contained in a small gap between two parallel nickel plates acting as electrodes. As a voltage difference is applied across the two electrodes, there is a redox reaction occurring on the electrode surfaces. Transport of the ions between the electrodes give rise to an electrical current which is measured by an ampere meter.

Potassium ferricyanide and potassium ferrocyanide are commonly used as redox ions in this electrochemical technique: ferricyanide ($Fe(CN)_6^{3-}$) is reduced to

ferrocyanide ($Fe(CN)_6^{4-}$ ) at cathode and ferrocyanide ($Fe(CN)_6^{4-}$) is oxidized to ferricyanide ($Fe(CN)_6^{3-}$) at anode, as shown in Figure 2.1.

$Fe(CN)_6^{3-} + e^- \rightarrow Fe(CN)_6^{4-}$ (cathode)

$Fe(CN)_6^{4-} \rightarrow Fe(CN)_6^{3-} + e^-$ (anode)

At steady state, ferricyanide transported to the cathode and ferrocyanide is transported to the anode due to concentration gradient and potential drop. An excess of an inert electrolyte, e.g. sodium hydroxide (NaOH) used in our experiments, is added to minimize the contribution of electrostatic fields to the total flux of ions. The total flux of ions is due to convection, diffusion and migration. The added $Na^+$ and $OH^-$ form double layers on the surfaces of the two electrodes. The double layer screen the electro field and make the migration of ion negligible. This is a widely used method to eliminate the migration contribution to the transport of the ions. Thus, with a large amount of electrolyte and stationary electrodes, the current produced by the redox ions is determined only by the rate of diffusion of the ions between the two electrodes. A plot of current versus voltage difference applied across the electrodes shows a limiting current which is related to the molecular diffusivity of the ions, as shown in Figure 2.2. When the voltage is low, the current increases with the voltage; when the voltage is higher than 0.4volts, the current reaches a constant value. This constant value of the current is called the limiting current. The reason for the existence of the limiting current is because when the voltage is low, the surface electrochemistry reaction is a control step and when the voltage is high enough, the diffusion of ions is a control step. Therefore, the limiting current is closely related to the molecular diffusivity of the ions while the electrodes are stationary.

At steady-state, with the same concentration of potassium ferricyanide and potassium ferrocyanide, the limiting current is related to the molecular diffusivity of ferrocyanide because when the concentration of ferricyanide and ferrocyanide is the

same, the limiting current is controlled by the smaller diffusivity of the redox ions. The diffusivity of ferrocyanide is about 10% smaller than that of ferricyanide (Arvia, 1976).

$$\frac{i_L}{nF} = \frac{SD}{H}(C_A - C_C) \qquad (2.1.1)$$

where $i_L$ is limiting current;

F is the Faraday constant;

n is the number of electrons transferred per ion oxidized or reduced (n=1 for ferricyanide and ferrocyanide redox ions);

H is the distance between the electrodes;

S is the cross-sectional area of electrodes;

D is the molecular diffusivity of ferrocyanide;

$C_A$ is ion concentration at anode;

$C_C$ is ion concentration at cathode.

Due to the symmetry of the electrode, the concentration of ferrocyanide at one electrode surface is two times of its initial concentration and is zero at the other electrode. So ($C_A$-$C_C$) can be simplified as 2C, where C is the initial concentration of potassium ferrocyanide.

$$i_L = \frac{2nFSDC}{H} \qquad (2.1.2a)$$

Equation 2.1.2a gives out the relationship between the limiting current and the molecular diffusivity when the two electrodes are stationary. When there is a particle suspension between the two electrodes and with two electrodes rotating, the mass transport of ions can be due to convection and diffusion. So in more general form, D is replace by $D^*$,

$$i_L = \frac{2nFSD^*C}{H} \qquad (2.1.2b)$$

Where $D^*$ can be molecular diffusivity, or hydrodynamic diffusivity or Maxwell diffusivity, or any combinations of these.

Therefore, the diffusivity of the redox ions can be calculated from the initial concentrations of the redox ions, the cell constant S/H, and the limiting current $i_L$. And Nusselt number can be calculated from the diffusivity and compared under different experimental conditions.

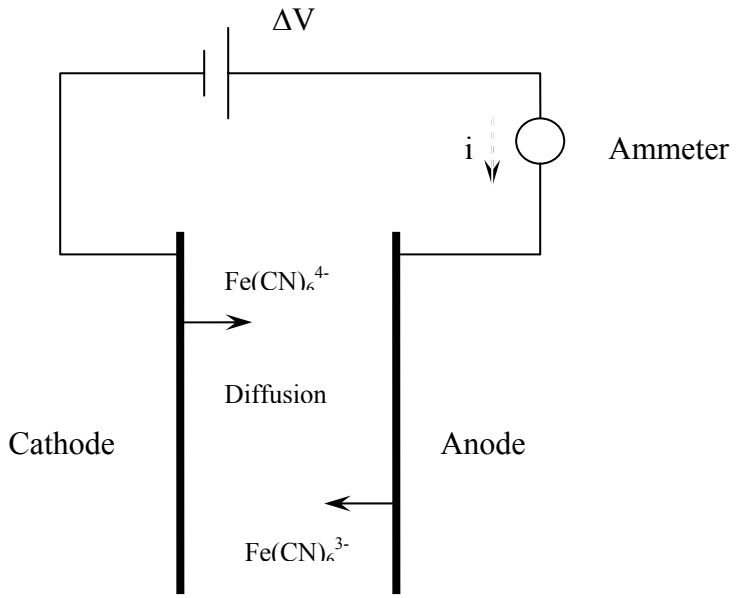


Cathode: $Fe(CN)_6^{3-} + e \rightarrow Fe(CN)_6^{4-}$ Anode: $Fe(CN)_6^{4-} \rightarrow Fe(CN)_6^{3-} + e$

Figure 2.1 Illustration of redox reactions of ferricyanide and ferrocyanide

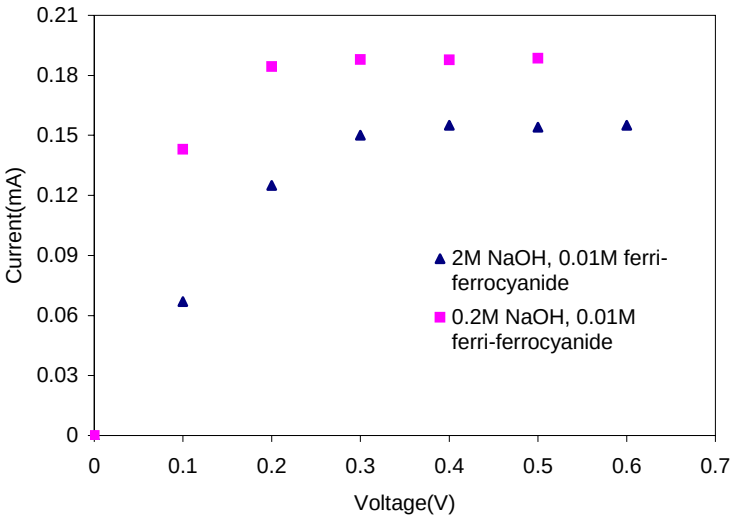


Figure 2.2. Steady-state diffusion current versus applied voltage. (The ratio of the viscosity of these two solution is 1.2).

A small cell was built to measure the diffusion of ions in the absence of shear. The schematic diagram of the small cell is shown in Figure 2.3. This small cell was composed of two parallel nickel plates mounted on Plexiglas® plates. The reason for choosing nickel is because the ferricyanide and ferrocyanide have fast redox reactions on the surface of nickel (Selman, 1978). The surfaces of nickel plates were polished to a mirror surface to delete oxidation film (Selman, 1978). All the experiments were carried out under a nitrogen environment to prevent oxidation at the nickel surface. The dimension of the plate was 20mm (width) × 30mm (length) × 1mm (thickness). The two nickel plates were spaced by two spacers. The thickness of the spacers was about 2mm. The nickel plates and the spacers were placed between two Plexiglas® plates and fixed by four plastic screws. The nickel plates were cut into the shape of wires at the upper end and connected to the circuit.

This small cell was left into the potassium ferricyanide and potassium ferrocyanide solutions. Two different solutions: solution A with 0.2M NaOH-17.5% (mass) glycery-0.01M potassium ferricyanide-0.01M potassium ferrocyanide and solution B with 1.22M NaOH-0.01M potassium ferricyanide-0.01M potassium ferrocyanide. With a potential drop across the two electrodes and connection to the circuit, the molecular diffusivity of ferrocyanide was measured. The diffusivity of ferrocyanide ion in the solution A was $3.24\times10^{-10}$ $m^2/s$ at 20 °C with a standard deviation of 8%; the diffusivity of ferrocyanide ion in solution B was $4.80\times10^{-10}$ $m^2/s$ at 20 °C with a standard deviation of 6%. The means of our measurements of the diffusivity are within 1% of those reported in the literature (Arvia, 1967).

The solution must contain a high enough concentration of the inert electrolyte (NaOH) to screen the electric field. If the concentration of NaOH is too low, electric field could have a significant effect on the limiting current because the current is not only due to the convection and diffusion, but also due to the migration. One way

of testing this is to determine that the diffusion mass flux of the redox ions is independent of the concentration of the inert electrolyte. Two experiments are shown in Figure 2.2. Two different concentrations of NaOH were tested for the same concentrations of ferricyanide-ferrocyanide: 0.2M NaOH-0.01M potassium ferricyanide-0.01M potassium ferrocyanide and 2M NaOH-0.01M potassium ferricyanide-0.01M potassium ferrocyanide. The limiting currents in these two solutions are 0.16mA and 0.19mA. The ratio of these two currents are comparable with that of the viscosity of these two solutions: 1.2. According to Arvia (1967), the diffusivity of ferrocyanide is inversely proportional to the viscosity of sodium hydroxide solution. So the difference between these two limiting currents is only due to the different viscosities. Taken into consideration of the viscosity difference, these two limiting currents are comparable with each other. This suggests that the concentration of NaOH does not have a significant effect on the limiting currents when concentration of NaOH is higher than 0.2M. Therefore, we conclude that 0.2M NaOH is high enough to screen the electric field for 0.01M ferricyanide-0.01M ferrocyanide redox reaction.

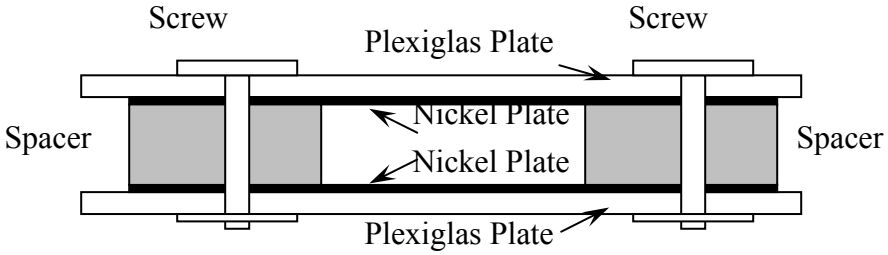


Figure 2.3 Schematic diagram of the small cell

### 1.1.2 Fluid-particle systems

Two sizes of monodispered polystyrene particles were used: 115μm and 230μm in radius. For mean radius of 115μm particles, 98.5% of particles were in the range of 106μm and 125μm as checked by the sieves; only 1.2% of particles were larger than 125μm and 0.3% of particles were smaller than 106μm. Five different volume fractions for each size of particles were studied: 0.1, 0.17, 0.25, 0.33 and 0.4. The particles were nearly neutrally buoyant in 1.2M NaOH. The experiments were conducted at room temperature 22 ± 1°C. Density of suspending medium at room temperature 22°C was $1.05\times10^{3}$kg/m$^{3}$. The concentration of potassium ferrocyanide and potassium ferrocyanide was 0.002M. The viscosity of suspending medium at 22 °C was $1.2 \times 10^{-6}$ m$^{2}$/s as measured by a viscometer in the shear rate range of 0 to 150 /second; Molecular diffusivity of ferrocyanide in this solution at 22°C is $5.5\times10^{-10}$m$^{2}$/s measured in the Couette cell. The Reynolds numbers of particles were up to 6.6 and Peclet numbers of particles were up to 15,870.

### 1.1.3 Couette cell design

The Couette cell was similar to the cell designed by N.L. Wang et al. (1978). In their design, the Couette cell consisted of two concentric cylindrical electrodes. The inner cylinder was about 4cm in diameter and 4.7cm in height. The gap between the electrodes was about 460μm. A copper sleeve on the outer cylinder remained in contact with a mercury bath during rotation which provided an electrical connection between the outer cylinder and the circuit. In our design, the Couette cell included two concentric hollow cylinders and each cylinder consisted of three sections: the middle section was made of aluminum coated with 100μm thick layer of electrodeposited nickel and the top and bottom sections of the cylinders were made of transparent Plexiglas®. The electrochemical reactions occurred on the middle section. The

transparent upper and lower sections of the cylinders allows the observation on the suspension inside of the Couette cell gap to assure the particles were uniformly suspended. The height of the metal parts was 12cm and of the Plexiglas® parts was 10cm. There were O rings which connected each Plexiglas and metal parts. The inner diameter of the outer cylinder was 12cm and the gap thickness was 5mm. The inner cylinder was stationary and the outer cylinder could be rotated from 0 to 120 rpm. A motor brush sitting on the top of the outer cylinder provided the electrical connection to the rest of the circuit when the outer cylinder was rotating. This design avoided to use toxic mercury for electrical connection between the outer cylinder and the circuit. Plexiglas® hollow flat ring attached on the top of the inner cylinder covered the gap between the two cylinders, as shown in Figure 2.5. A high purity nitrogen gas was injected into the hollow channel of this flat cover between the two cylinders and then flowed out from six holes into the gap of the Couette cell and remained on the surface of the particle suspension, providing nitrogen blanket during the whole experimental process.

The electrical circuit was built as shown in Figure 2.4. A conducting Cu wire connected the stationary inner cylinder to a steady power supply and then to an ampere meter. The circuit was completed by connecting the motor brush to the outer cylinder. The ampere meter also connected to a computer, transferring all the current data to the computer for later data analysis.

The geometry of the Couette was designed to minimize the secondary flows. The inner cylinder was stationary and the outer cylinder rotating so that the Taylor-Couette instability did not occur. In addition, a large value of the Couette height to gap thickness ratio was also desired to minimize secondary flows.

Even with the inner cylinder stationary and outer cylinder rotating, the Couette flow undergoes a transition to turbulence. The transition occurs for a Reynolds number

based on the gap thickness $\mathrm{Re}_H = \dot{\gamma} H^2 / \nu$ at about 5,500 for our Couette cell with r/R=0.917, where r is the radius of the inner cylinder and R is the radius of the outer cylinder (Schlichting, 1955). The shear rate is defined as the speed of the outer cylinder divided by the gap thickness of the Couette cell. Our experiments span a range of $\mathrm{Re_H}$ = 0-3,125. All of the experiments were performed under conditions where the single-phase flow in the Couette was stable.

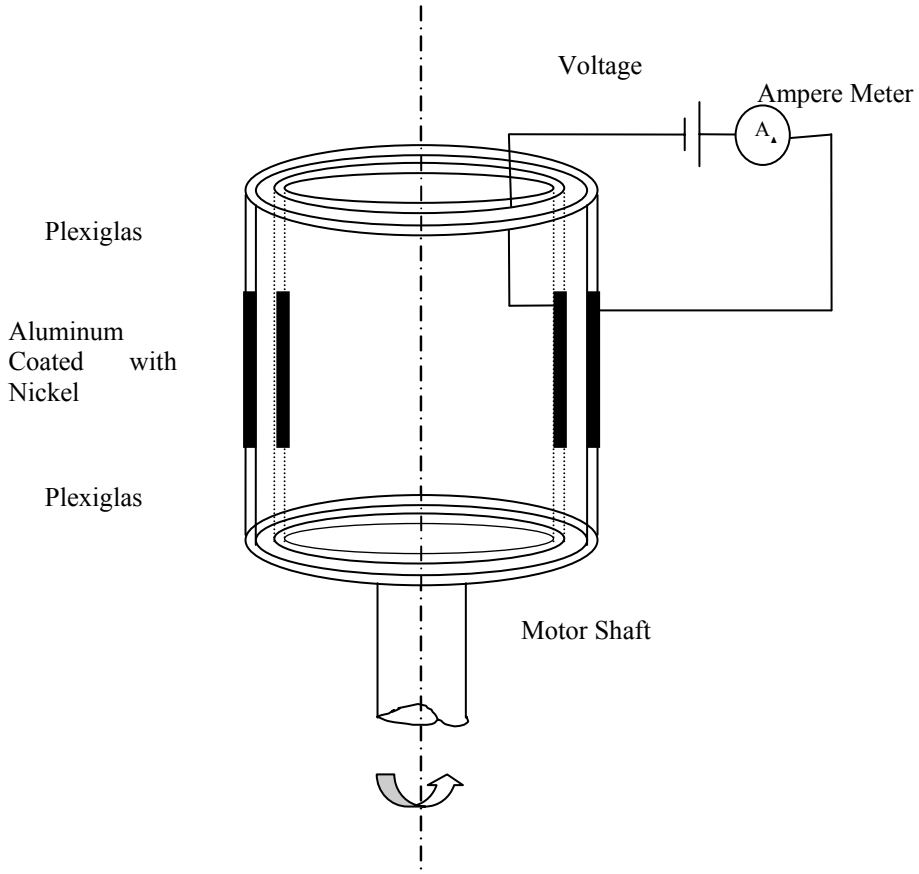


Figure 2.4. The diagram of the Couette cell

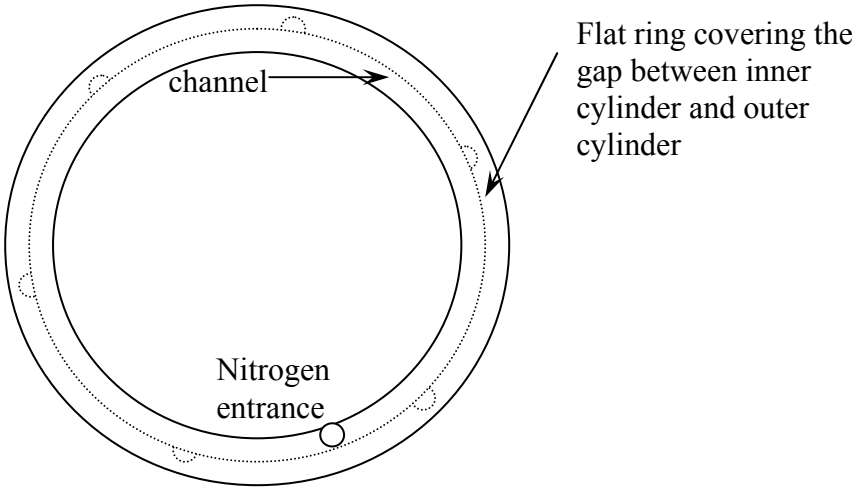


Figure 2.5. Top view of flat ring providing a nitrogen blanket on top of the solution between the cylinders.

### 1.1.4 Experimental procedure

Since nickel can be oxidized by oxygen, the two electrodes were polished by micro-sized sand paper to remove oxidation thin layers at regular intervals. The system was aligned with the aid of a dial indicator. First, the three sections of each cylinder were aligned to be parallel to each other. Then the vertical positions of the inner and the outer cylinder were adjusted to achieve concentricity. The accuracy of all adjustments was on the order of 200 μm.

The suspension solution of 500ml was bubbled by high purity nitrogen for thirty minutes before each experiment to remove any oxygen in the solution because oxygen can react with nickel and affect the limiting currents. The suspensions were sonicated for 15 minutes to remove bubbles in the suspension. Then the suspension was left in the vacuum oven for about 10 minutes to remove the bubbles generated by the nitrogen bubbling. In addition, the suspension solution was under nitrogen blanket during the whole experimental process. After the suspension solution was introduced into the Couette cell, the outer cylinder was rotated at desired speeds, varying from 0 to 120 rpm. A potential drop of 0.4 volts was applied across the two electrodes and the current was continuously recorded and transferred to the computer for later analysis. All the experiments were run at room temperature, 22 ± 1 °C.

## 1.2 Experimental Results and Discussion

The Nusselt number represents the enhancement of mass transport due to the shear flow. The non-dimensional numbers Nu, Pe and Re are defined as

$$Nu = \frac{hH}{D} \tag{2.1.3}$$

$$Pe = \frac{\dot{\gamma} a^2}{D} \tag{2.1.4}$$

$$\mathrm{Re} = \frac{\dot{\gamma} a^2}{\nu} \tag{2.1.5}$$

where h is mass transfer coefficient in the sheared suspensions;

H is the gap thickness of the Couette cell (H=5 mm in our experiments);

D is the molecular diffusivity;

$\dot{\gamma}$ is the shear rate;

a is the particle's radius;

ν is the kinematic viscosity.

Acording to equation 2.1.2b, the limiting current is proportional to the effective diffusivity. So Nu, defined as $Nu = hH / D = D^* / D$, can be calculated from the equation:

$$Nu = \frac{i_L H}{2nFSCD} \tag{2.1.6}$$

So as long as the limiting current is known, the Nusselt number can be calculated from it for different experimental conditions.

The diffusivities in the stationary suspensions ($\dot{\gamma}$ = 0) were measured and compared with the results of Maxwell equation. And the mass transfer rate was also measured in sheared suspensions in which particle radii were 115 μm and 230 μm at five different volume fractions, 0.1, 0.17, 0.25, 0.33 and 0.4, with Re up to 6.6 and Pe up to 15,870.

1.2.1 Stationary Suspensions ($\dot{\gamma}$ = 0)

To investigate whether the Couette cell works well, limiting currents in stationary suspensions were measured. The effective diffusivity of the suspensions was calculated from equation 2.1.2b. The theoretical predictions for this ratio as a

function of particle volume fraction and molecular diffusivity in the particle, $D_P$, is described below. They are compared with the results presented here.

Maxwell (1892) first reported a theoretical estimate of the effective diffusivity of a stationary suspension of randomly dispersed spheres as follows:

$$\frac{D^* - D}{D^* + 2D} = \Phi \frac{D_{PP} - D}{D_{PP} + 2D} \tag{2.1.7}$$

Where

$D^*$ is the diffusivity in the particle suspensions;

D is the diffusivity in the suspending medius;

$D_{PP}$ is the diffusivity in the particle phase;

$\Phi$ is the particle volume fraction;

For a diffusing species with negligible diffusivity in the particle phase, i.e., $D_{PP}/D \rightarrow 0$, the above equation simplifies to

$$\frac{D^*}{D} = \frac{1 - \Phi}{1 + \frac{\Phi}{2}} \tag{2.1.8}$$

Maxwell equation is rigorously valid for $\Phi << 1$. However, it has been found from experiment and numerical simulation to work very well for $\Phi$ as high as 0.6 if $D_{PP}/D \rightarrow 0$ (Turner, 1976 and Bonnecaze and Brady, 1991).

Two sizes of particles, radius 115μm and 230μm, were used and five different particle volume fractions, 0.1, 0.17, 0.25, 0. 33 and 0.40, were studied and compared with Maxwell equation. The results are shown in Figure 2.6.

The experimental data are very close to the Maxwell theoretical prediction. This indicates the measurement principle and procedures were working well. Also, it indicates that the particles were well density matched with the fluid because any settling or floating due to density mismatch would have a strong effect on the mass

transfer. From the observations through the transparent Plexiglas®, the particle suspensions were homogeneous and not aggregating. Therefore, this system is reliable for the investigation of mass transfer rate in sheared neutrally buoyant particle suspensions.

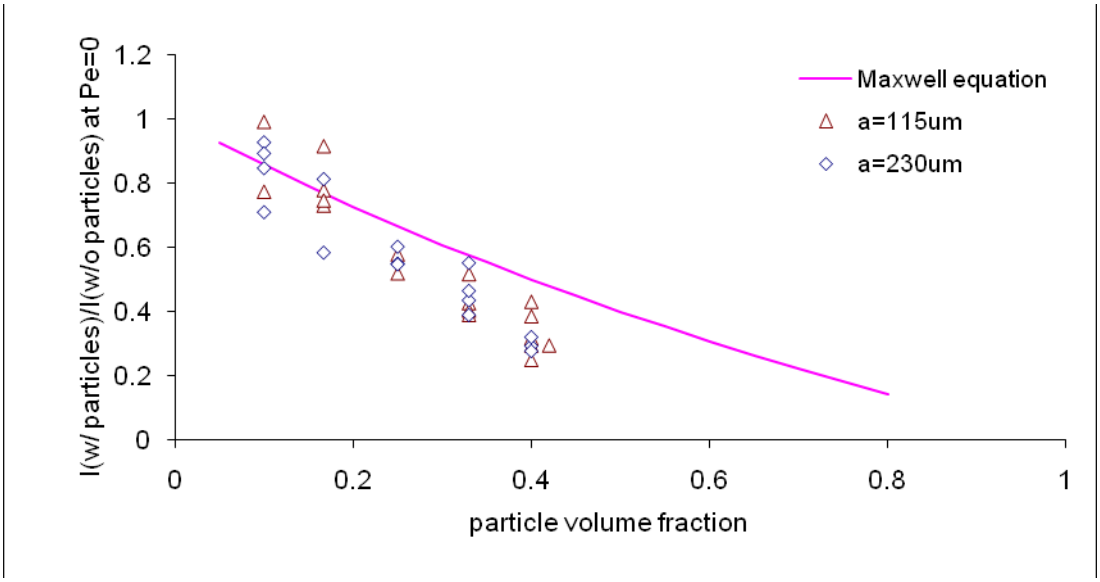


Figure 2.6. Comparison of diffusivity in stationary suspensions with Maxwell predictions.

### 1.2.2 Sheared Suspensions

Mass transfer process in sheared neutrally buoyant particle suspensions was studied at five different volume fractions: Φ=0.1, 0.17, 0.25, 0.33 and 0.4 at varying rotation speeds of outer cylinder from 10 rpm to 120 rpm. Particles used in these experiments were spherical monodispersed polystyrene and their radii were 115μm and 230μm. These conditions led to a maximum of Re=6.6 and Pe=15,870.

The limiting currents under different rotation speeds at volume fraction Φ=0.17 are shown in Figure 2.7. The order of rotation speed was randomly chosen and the results show that the order does not have any effect on the final results. At the highest rotation speed, 120 rpm, the limiting current is almost ten times larger than that in quiescence. This clearly indicates that the mass transfer is significantly increased in sheared suspensions.

Nu is calculated according to equation 2.1.6 with standard deviations estimated from four or five runs of repeated experiments. The values of Nu are plotted as a function of Peclet number at different volume fractions for particle radius 230 μm in Figure 2.8 and for particle radius 115μm in Figure 2.9. Because gap thickness of the Couette cell (H) in the experiments was 5 mm, H/a values for radii 230 μm and 115 μm particles were 22 and 44, respectively.

From Figure 2.8 and Figure 2.9, it can be seen that mass transfer rate increases with shear rate. For smaller particles, at lower Peclet number, the Nu is almost linear with Pe. For larger particles, at high Peclet number, Nu increases at a lower rate.

It can also be seen that at any given Peclet number, Nusselt number increases with Φ from Φ=0.1 to Φ=0.4. But at higher volume fractions, the increase rate becomes slower. This can be seen from the fact that Nu is very close for 0.33 and 0.4, but larger difference for 0.1 and 0.17.

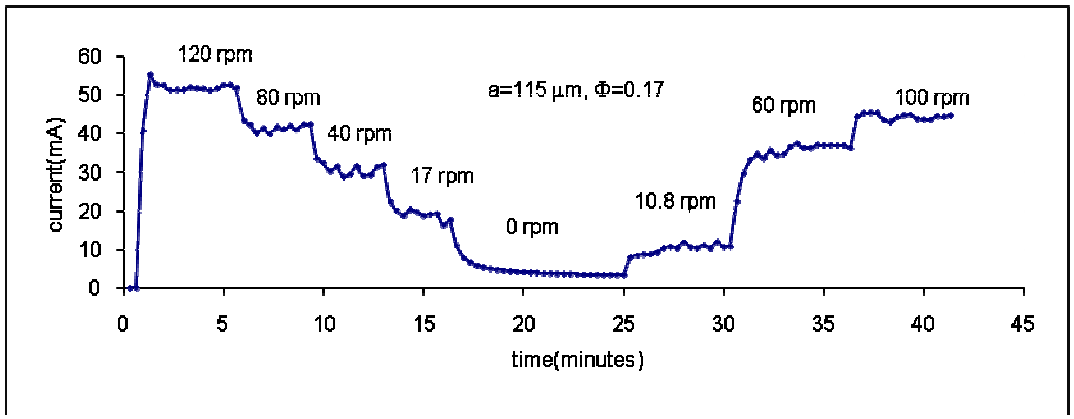


Figure 2.7. Limiting currents under different rotation speeds at Φ=0.17

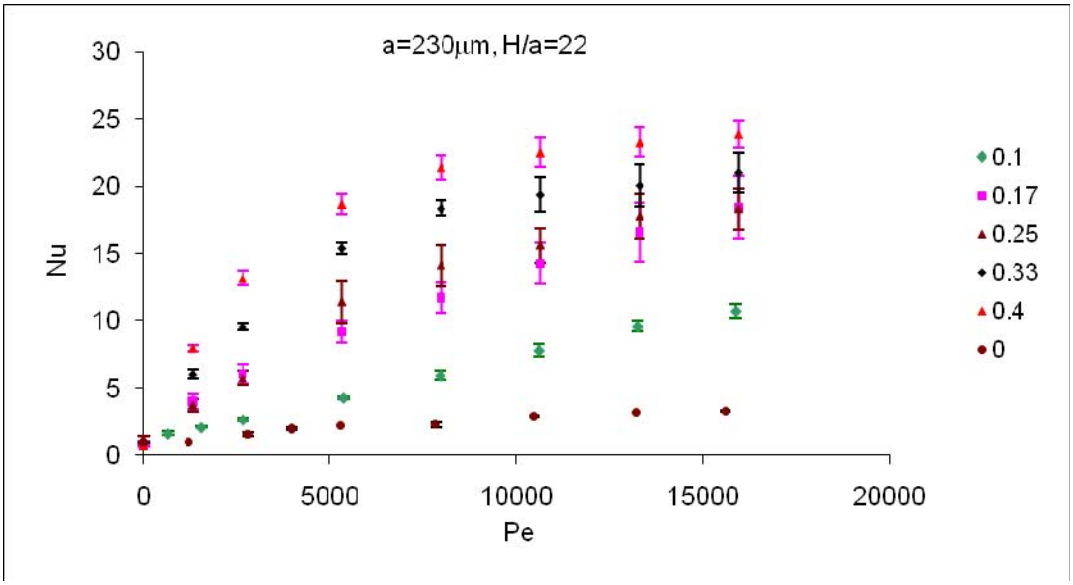


Figure 2.8. The Nusselt number in the sheared suspensions for radius 230 μm particles at different volume fractions.

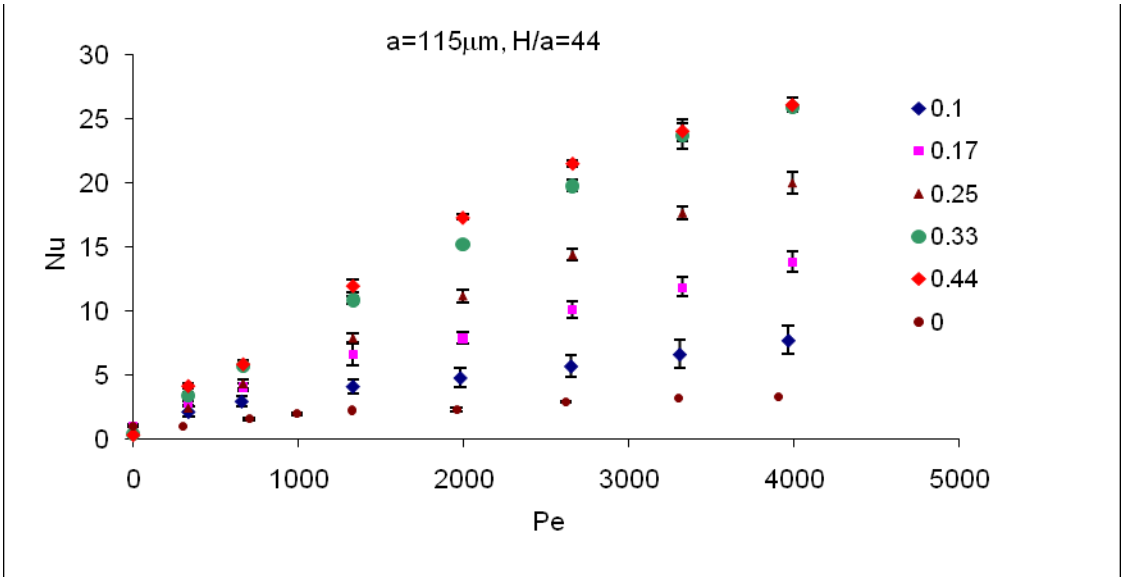


Figure 2.9. The Nusselt number in the sheared suspensions for radius 115 μm particles at different volume fractions.

To test the possibility of other (secondary) flow effects may have on the mass transfer, experiments were performed without particles (Φ=0) at different rotation speeds, as shown in Figure 2.10. The purpose of these experiments was to evaluate the contribution of other flow effects to mass transfer increase. At the highest rotation speed, 120 rpm, corresponding to Pe=3960 for smaller particles and Pe=15,870 for larger particles, the increase in measured current due to secondary flow effects is almost two times that measured for the stationary suspending medium. However, compared to the increase due to the random motion of the fluid induced by the particles, almost 25 times for 0.4 volume fraction and 10 times for 0.1 volume fraction, this effect is small and can be neglected. Therefore, the mass transfer increase in the Couette cell subjected to a shear flow is mainly due to the random motion of the fluid induced by the presence of the particles. Other effects were small enough to be neglected.

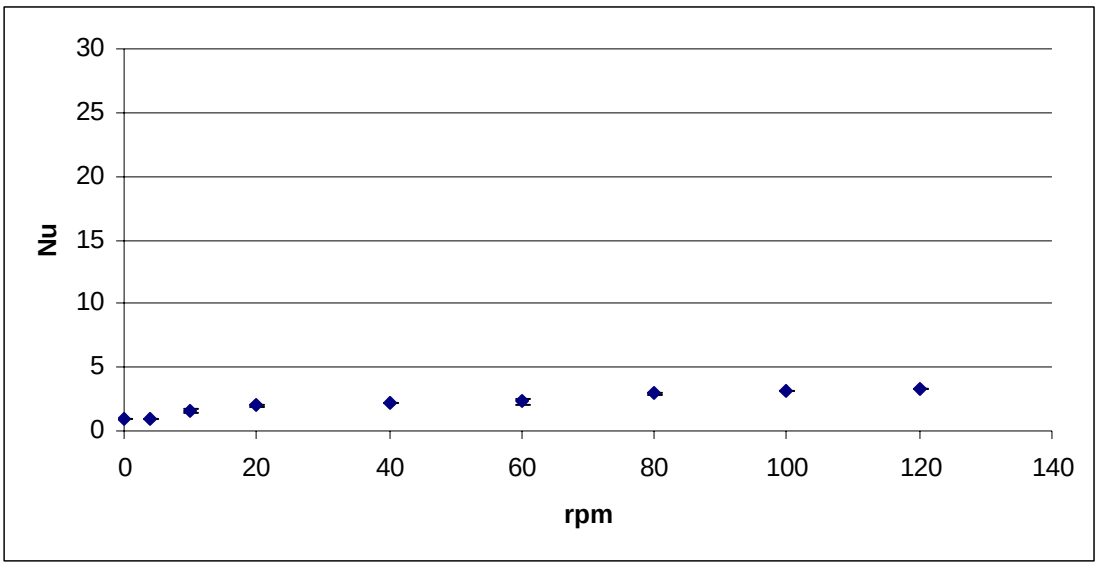


Figure 2.10. Investigation of secondary flow effects on the mass transfer in the absence of particles (Φ=0).

2.2.3 Sheared Suspension Results Compared with previous experimental work (Wang & Sohn)

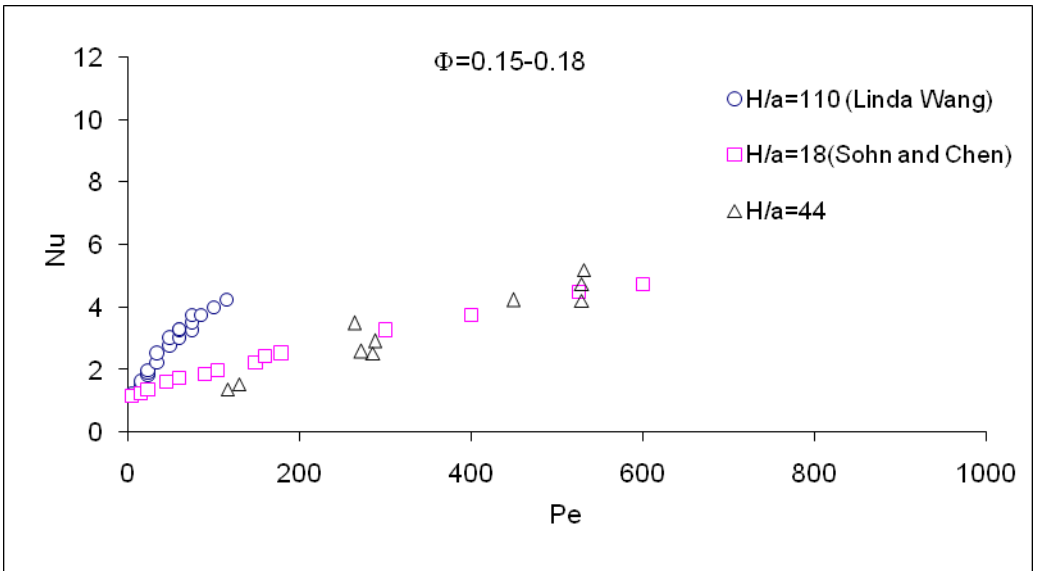


Figure 2.11 Comparison with previous experimental results (Wang and Sohn) for Φ =0.15-0.18

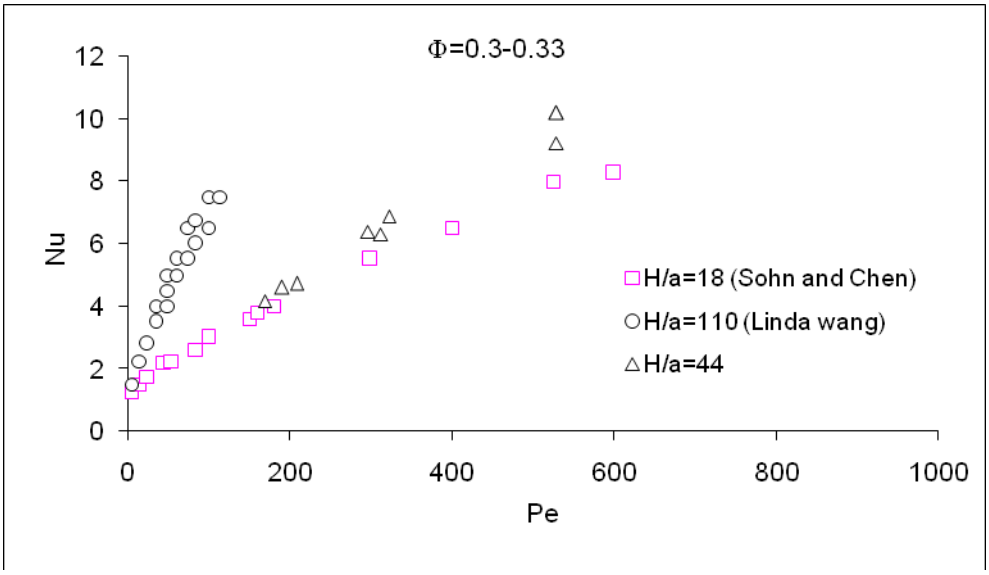


Figure 2.12 Comparison with previous experimental results (Wang and Sohn) for Φ=0.3-0.33

Our results are compared with corresponding previous experimental studies by Wang & Keller and by Sohn and Chen in Figure 2.11 and Figure 2.12. Our values for Nu are smaller than those of Wang and Keller and comparable with those Sohn and Chen's results for both 0.17 and 0.33. Since our H/a is 44 which is in between of H/a=110 and H/a=18, values of Nu in our system are expected to be in between those of Wang & Keller and those Sohn & Chen. The reason for our results being comparable with those of Sohn & Chen could be due to the difference between heat transfer and mass transfer. In the solid-liquid systems, mass can only be carried through liquid phase, but heat can be carried by both the liquid phase and the suspended solid phase. So the heat transfer rate in Sohn & Chen's experiments is expected to be larger than our mass transfer rate. In most solid-liquid systems, the heat capacities of liquid and solid are comparable, which is also true in Sohn and Chen's case: the heat capacity of the polystyrene is $1.19\times10^{-3}$J/Kg K and that of the mixture oil is $1.46\times10^{-3}$J/Kg K. So this heat transfer and mass transfer difference affects quantitative results, but not the qualitative trends.

## 2. Simulation and Results

### 2.1 Simulation Introduction

We performed simulations to study mass transfer increase due to the random fluctuation of fluid induced by the particles in neutrally buoyant particle suspensions. The effects of Φ, H/a, Pe and Re were studied. The advantages of simulation over experiments are that we can get tracer concentration profile directly from simulation. From the concentration profile, the mass transfer coefficient in bulk region and boundary layers can be determined separately. And also, inertial effect and shear rate effects can be studied independently in simulation, while in experiments, with increasing shear rate, Pe and Re both increase.

The simulations were conducted using lattice-Boltzmann method developed by Ladd (Ladd, 1994a, b, 2001). The solution of the governing Navier-Stokes equations is obtained as a consequence of propagating fluid particles. In the lattice-Boltzmann method the system is characterized by the velocity distribution function at lattice nodes. And then the macroscopic quantities, e.g. mass, momentum and stress, can be obtained from the moments of the velocity distribution function. In this study, we used a three-dimensional 19-velocity model, including the zero-velocity (staying at the current lattice position) and the vectors connecting each node with its nearest and next-nearest neighbors on a cubic lattice. The update of the velocity distribution function includes collision and propagation. In the collision step, the populations of fluid molecules at each lattice node are rearranged in such a way that mass and momentum conserve and the velocity distribution function relaxes to a local equilibrium. In the propagation step, the fluid molecules travel to the neighboring lattice nodes according to the velocity distribution after collision. Fluid molecule populations that are moving from a fluid node to a solid node are bounced back towards the node they came from with their values modified to account for the velocity of the boundary. The effective hydrodynamic diameter is determined by comparing the lattice-Boltzmann simulation results for the steady-state drag due to Stokes flow through a cubic array of spheres to the corresponding analytical results (Sangani, 1982). The effective hydrodynamic diameter is only dependent on the input diameter and viscosity. The input and effective diameters used in this study were 2.72 and 2.92 which were determined by averaging simulation results for 5 to 7 randomly chosen positions of the particle relative to the lattice (Yin, 2006). These values give good accuracy for sedimentation at Re=0.5 – 20 (Yin, 2006). When the particles are very close to each other, the lack of fluid nodes between the particle's surfaces results in a breakdown of the short-range lubrication force. This breakdown is caused by the

finite resolution of the grid. When the gap between the particle's surfaces becomes smaller than a critical value, the lubrication force is a constant and only a function of fluid viscosity and lattice spacing. Since the lubrication force is known analytically, this lubrication force breakdown is corrected by adding an interparticle force when the gap is smaller than the critical value (Ladd, 2001).

We used a tracer method to simulate the transport of ions in the flow field. It has been shown that the convection-diffusion process of passive species (solute, ions, etc.) in a flow field can be modeled by the motion of tracers governed by the Langevin equation. The Langevin equation for tracer particles, implemented using a forward-Euler scheme, is of the form

$$\mathbf{r}(t+\Delta t) = \mathbf{r}(t) + \mathbf{v}[\mathbf{r}(\mathbf{t})]\Delta t + \xi\sqrt{6D\Delta t}\ ,$$

where **r** is the position vector, **v(r)** is the fluid velocity at current tracer location obtained by linearly interpolating the velocity field from lattice-Boltzmann simulation, and $\xi$ is a vector with a random orientation but a constant length 1. There are two common choices for the random displacement. One could have a Gaussian variable for the displacement which would have the advantage that the displacements would be Gaussian for any interval of time. This is a common choice. However, it has the disadvantage that in rare cases the step may be very large causing the particle to cross the gap or go deep into a particle or have multiple reflections from particles and/or walls. Our choice of a constant step limits the step size and avoids these problems. The displacement will still be Gaussian after many times $\Delta t$ but not each $\Delta t$ interval. These tracers undergo Brownian diffusion as well as being convected by the fluid velocity field computed by the lattice-Boltzmann method. If **r** ($t + \Delta t$) enters a solid boundary, a specular reflection is performed to ensure that tracers do not permeate the solid particles. The tracers and the solid particles are both moved at the same time before

the check for collisions and the reflection is implemented. This tracer method is able to give the time averaged flux and concentration profiles as function of y without needing a small spatial grid to resolve boundary layers but only a small enough time step. Although this method does not provide enough statistics to know the detailed concentration field at every instant of time if one needed that, fortunately this is not necessary to interpret our experiments. This tracer method is sometimes referred to as the particle-tracking method in the literature, and is particularly useful for moderate-to-high Peclet number flows because it does not require a refined computational grid to resolve the diffusion boundary layers.

In this work, our simulation geometry consisted of a suspension of spherical particles confined between two planar walls moving in opposite directions with same speed. There were two types of tracers in the simulations referred to as type A and B. Initially, tracers of type A and those of type B were randomly distributed in the fluid and intimately mixed. In order to simulate the redox reaction of ions in the Couette cell experiment, we designed tracer collision rules such that when a tracer of type A collides into wall I, it was specularly reflected and converted into a tracer of type B, and when a tracer of type B collides into wall II, it was specularly reflected and converted into a tracer of type A. The instantaneous exchange of tracer A to B or vice versa modeled the case where there is no surface reaction kinetic limitation which was also the situation for the experiment. Whenever tracer A collides with wall II and tracer B collides with wall I, they are specularly reflected and without conversion. Over time, a boundary layer with high concentration of A and low concentration of B will develop near wall II; similarly, a boundary layer with high concentration of B and low concentration of A will develop near wall I. After the transport of tracers reaches a steady state, the equilibrium flux of tracers across the gap can be obtained from the average number of tracer conversions per unit time. The overall mass transfer

coefficient in the Couette cell can thus be determined using the flux and the concentration difference of tracers across the gap. The concentration of tracer A at the wall I and the concentration of tracer B at the wall II are zero. By symmetry, the concentration of tracer A at the wall II and the concentration of tracer B at the wall I are two times of the initial concentration of A or B. In addition, the time-averaged concentration profiles for tracers A and B obtained from simulations can be used to assess the relative importance between the mass transfer resistance in the bulk suspension and that in the boundary layers near the walls.

Our computational domains were rectangular in shape and were bounded by a pair of solid walls as in an experimental Couette cell. In addition to the solid walls, we applied periodic boundary conditions in the other two directions, defined as x and z directions. The distance between solid walls, defined as y direction, was set to approximately 5, 7.5, and 10 times of the particle diameter (6 lattice units) in our simulations. The size of the computational domain in the other periodic directions was set to approximately 5 times of the particle diameter. The density and viscosity of the fluid expressed in lattice unit were 36 and 0.36. This relatively low viscosity of the fluid allows us to achieve moderate particle Reynolds numbers without incurring significant errors from the compressibility of the fluid. The density of particles is the same as the fluid, making them neutrally buoyant as in the experiments.

## 2.2 Simulation Results

Simulations were conducted at three different solid particle volume fractions, 0.1, 0.17 and 0.25. The effect of the ratio of gap thickness to particle radius (H/a) on mass transport was investigated at Re=0.5. The reason we chose Re=0.5 is that the simulation cost increases with decreasing Re if Re is small and that we expect Re=0.5

to be small enough to show approximately the small Re behavior. Larger Reynolds number, e.g. Re=1.5, was also conducted to study inertial effect.

Inertial migration of particle might occur at lower volume fraction and may have effects on the mass transfer rate. This effect is also studied numerically. Smaller Reynolds numbers simulations, e.g. Re=0.1 and Re=0.25, were conducted for volume fraction 0.1 since it was expected that migration rate depends on Reynolds number.

### 2.2.1 Nusselt Number as Function of Peclet Number for Different Particle Volume Fractions and Different H/a

The Nusselt number as a function of the Peclet number, volume fraction and ratio of gap thickness to particle radius (H/a) has been shown in Figure 2.13, Figure 2.14 and Figure 2.15 for 0.17, 0.25 and 0.1. For all the volume fractions and H/a, the Nusselt number increases with Peclet number. For all the volume fractions, 0.1, 0.17 and 0.25, at any given Peclet number, Nusselt number increases with H/a, from H/a=10 to H/a=20. And at any given H/a, e.g. H/a=15, Nusselt increases with volume fraction, as shown in Figure 2.16. From volume fraction 0.1 to 0.15, Nusselt number increases faster compared to the increase from 0.17 to 0.25. All these trends qualitatively agree with Koch theory (1996). Higher volume fraction gives larger hydrodynamic diffusivities according to Koch theory, smaller H/a gives more boundary layer resistance and higher Peclet number gives higher hydrodynamic diffusivity.

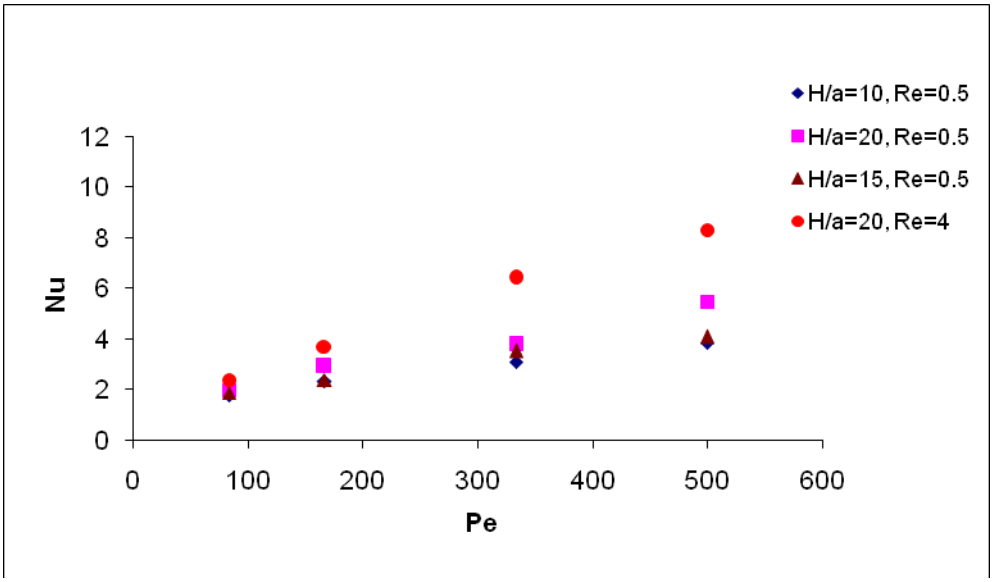


Figure 2.13 Nusselt number as function of Peclet number and H/a for Φ=0.17.

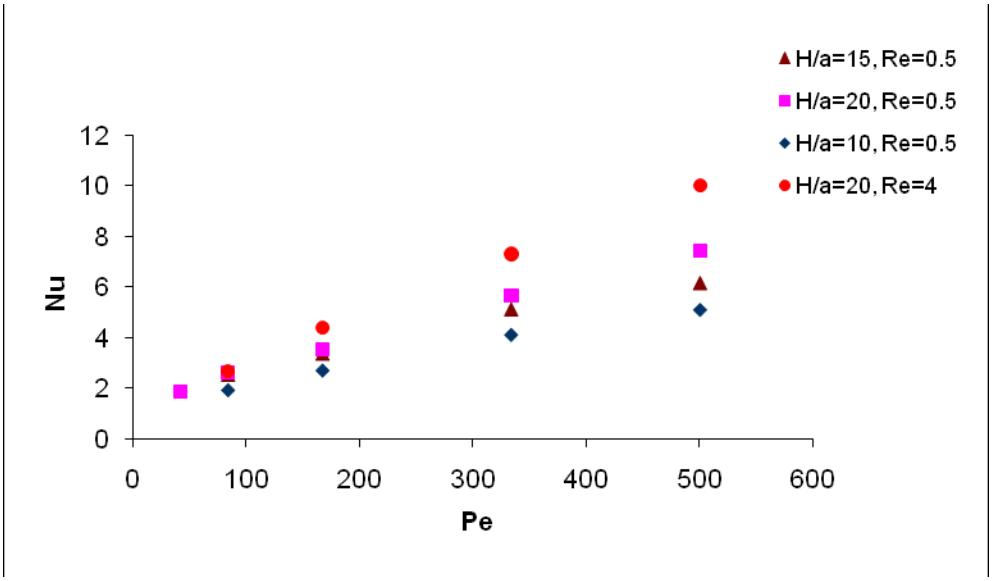


Figure 2.14 Nusselt number as function of Peclet number and H/a for Φ=0.25.

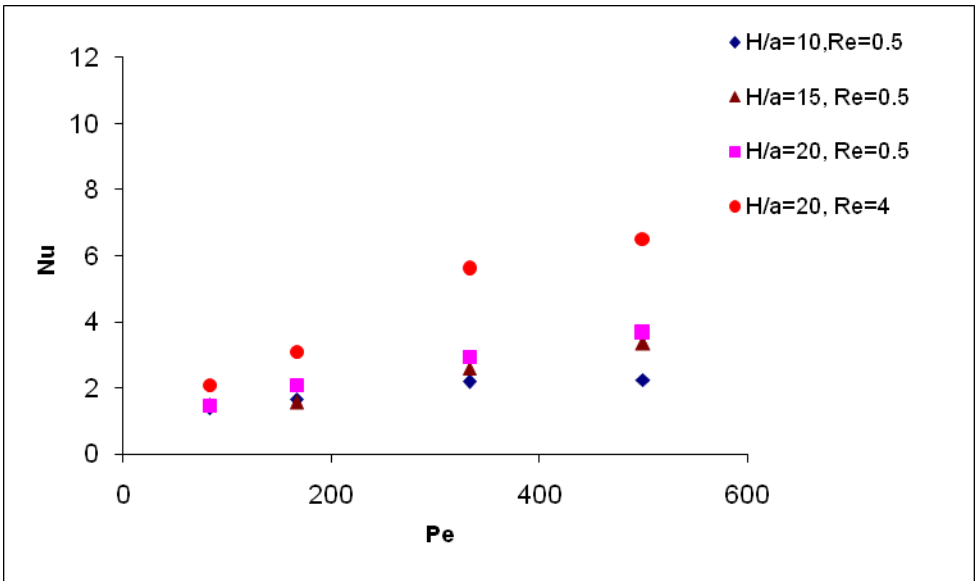


Figure 2.15 Nusselt number as function of Peclet number and H/a for Φ=0.1.

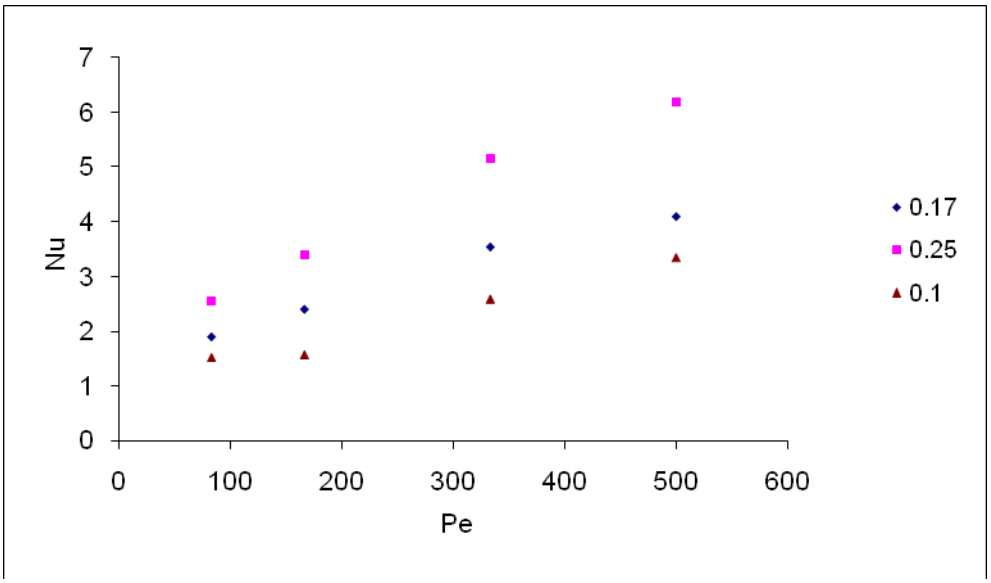


Figure 2.16 Nusselt as function of Peclet number for different volume fractions at H/a=15.

### 2.2.2 Inertial Effect on Mass Transport

Since the fluid velocity fluctuations are likely to be enhanced at higher Reynolds numbers, the inertial effect was studied at 0.17. Different Reynolds number simulations were conducted and results are shown in Figure 2.17. Results shows that Nusselt number is almost a linear function of Reynolds number from Re=0.5 to Re=10 except there is some leveling off at the smaller Reynolds number (More points are coming out to show this better). This relationship is used for later comparison of simulation results with experimental results since simulation was conducted at constant Reynolds number and experiments results were under different Reynolds number for different Peclet numbers.

### 2.2.3 Velocity Profile, Concentration Profile

The time-averaged fluid velocity and tracer concentration profiles were calculated and steady-state profiles are shown in Figure 2.18 and Figure 2.19. The velocity slip and concentration slip are listed in Table 2.1 for different Re, volume fractions and H/a. The concentration profile and velocity profile both show that at steady-state there are two regions in the gap between two walls: bulk region and boundary layers. In the bulk region, the concentration gradient is small and a constant; the velocity gradient is a constant. In the boundary layer region, there is a concentration slip and velocity slip. The slip is defined as the difference between the concentration or velocity at the wall and the concentration or velocity extrapolated from the bulk region, middle 1/3 of the region, by fitting straight line. The velocity slip is due to the depletion of the particle near the walls. The concentration slip could be the results of two effects: no-slip boundary condition and depletion layers of particles near the walls. The no-slip boundary condition requires the fluctuating velocity to decrease near the wall. It is noted from the velocity profile that the bulk shear rate is not the same as wall velocity divided by the gap thickness. But we still

use this crude measure of shear rate in defining Reynolds number and Peclet number which is consistent with what we do in the experiments where we cannot detect a bulk shear rate.

### 2.2.4 Volume Fraction Distribution

The depletion of particle near the walls can also be shown from the particle volume fraction distribution, as shown in Figure 2.20 (a, b, c) for 0.10, 0.17 and 0.25 respectively. For 0.17 and 0.25, in the bulk region, volume fraction is more than the average volume fraction and in the boundary layers volume fraction is lower than the average. There was depletion region of particles near the wall causing concentration slip. The depletion layer thickness is defined as

$$\delta_D = H(1 - \langle \Phi \rangle / \Phi_b)/2$$

Where $\delta_D$ -- depletion layer thickness;

$\langle \Phi \rangle$ -- average volume fraction;

$\Phi_b$ – bulk volume fraction;

The bulk volume fractions and depletion layer thickness for different Re, average volume fractions, and H/a are listed in Table 2.2. The depletion layer thickness is comparable with radius of particle. For $\Phi$=0.1, as shown in Figure 2.20 (a), 2.21 (a) and (b), there is a much larger depletion region near the walls. This could be due to migration of particles at lower volume fractions. Particle-wall interaction causes particles migrate away from the walls. Particle-particle interaction keeps the particles distributed uniformly. At lower volume fraction, e.g. $\Phi$=0.1, particle-particle interaction is weaker compared with that at higher volume fraction, e.g. $\Phi$=0.17 and 0.25. So migration of particles is expected to be seen at lower volume fractions. More detailed discussion can be found in chapter 4.

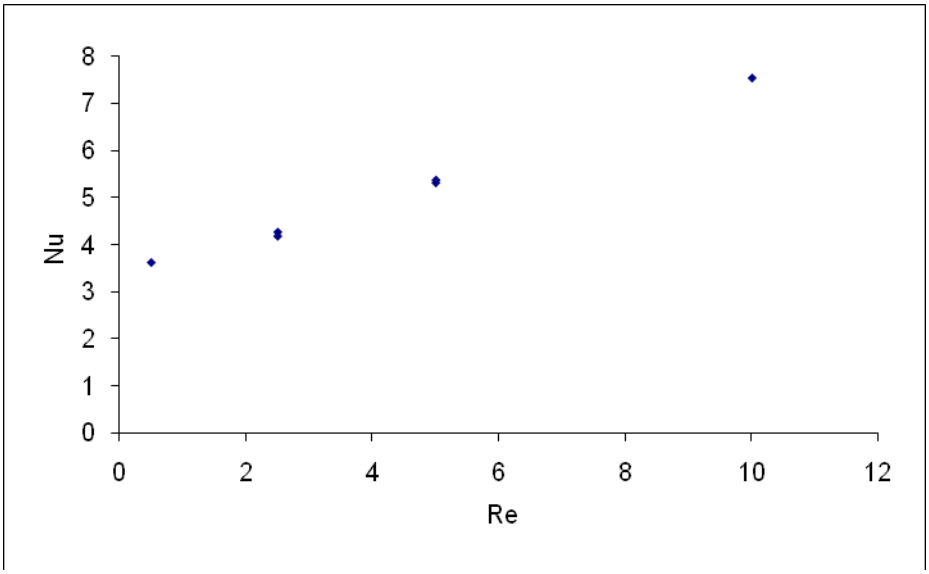


Figure 2.17 Nusselt number as function of Reynolds number at Φ=0.17 and H/a=10.

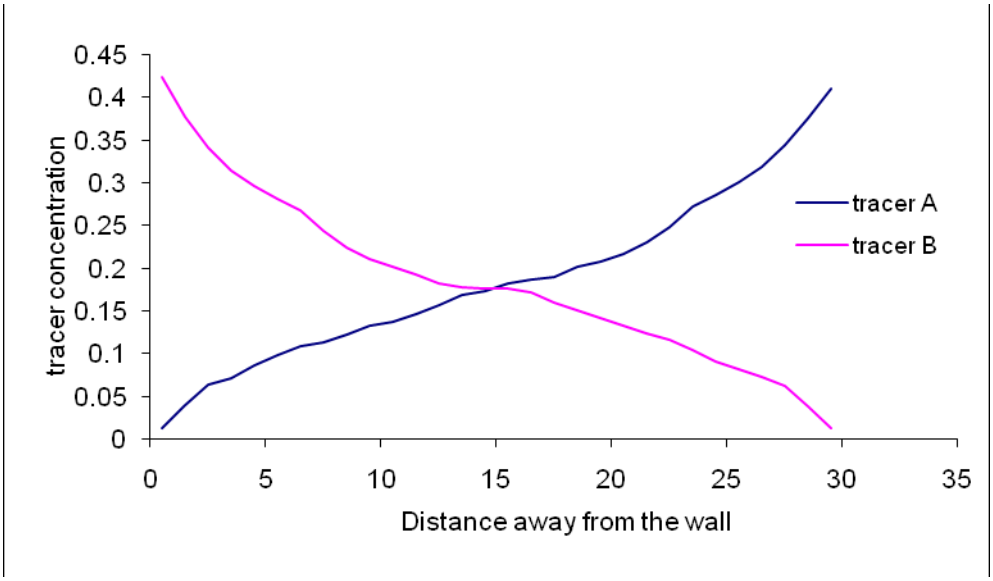


Figure 2.18 Tracer concentration profile for Φ=0.17, Pe=166.7, H/a=10 and Re=0.5.

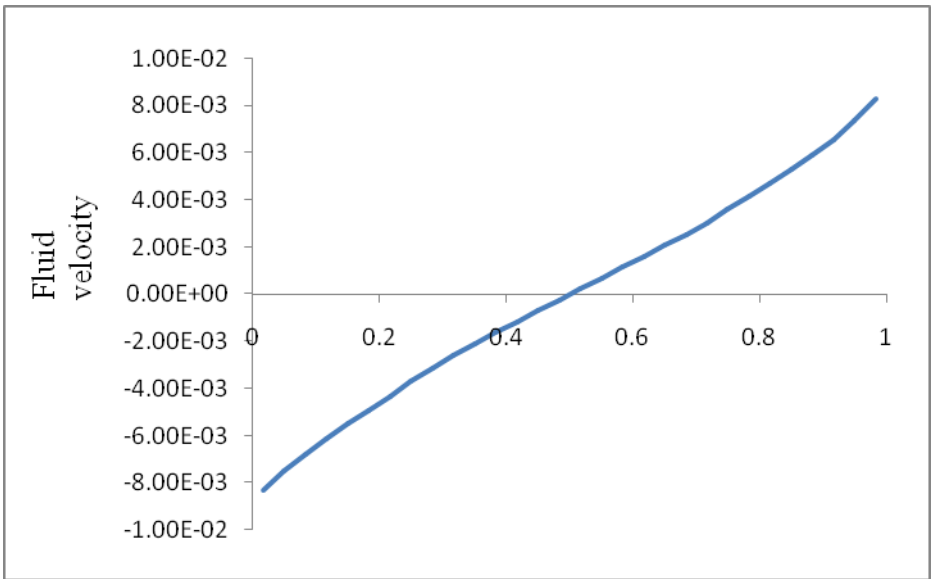


Figure 2.19 Velocity profile at Φ=0.17, Pe=166.7, H/a=10 and Re=0.5.

Table 2.1 The velocity slip and concentration slip for different Re, volume fractions and H/a.

| Re | Volume fraction | H/a | Concentration slip/Cinitial | Velocity slip |
|---|---|---|---|---|
| 0.5 | 0.1 | 10 | 4.72E-01 | 1.40E-03 |
| | | 15 | 3.90E-01 | 1.55E-03 |
| | | 20 | 3.00E-01 | 1.84E-03 |
| | 0.17 | 10 | 3.66E-01 | 1.13E-03 |
| | | 15 | 3.21E-01 | 2.00E-03 |
| | | 20 | 3.11E-01 | 2.24E-03 |
| | 0.25 | 10 | 5.76E-01 | -1.5E-4 |
| | | 15 | 4.65E-01 | 8.00E-04 |
| | | 20 | 4.37E-01 | 2.70E-03 |
| 4 | 0.1 | 20 | 2.17E-01 | -8.6E-03 |
| | 0.17 | 20 | 2.43E-01 | -9.0E-03 |
| | 0.25 | 20 | 3.26E-01 | -1.0E-03 |

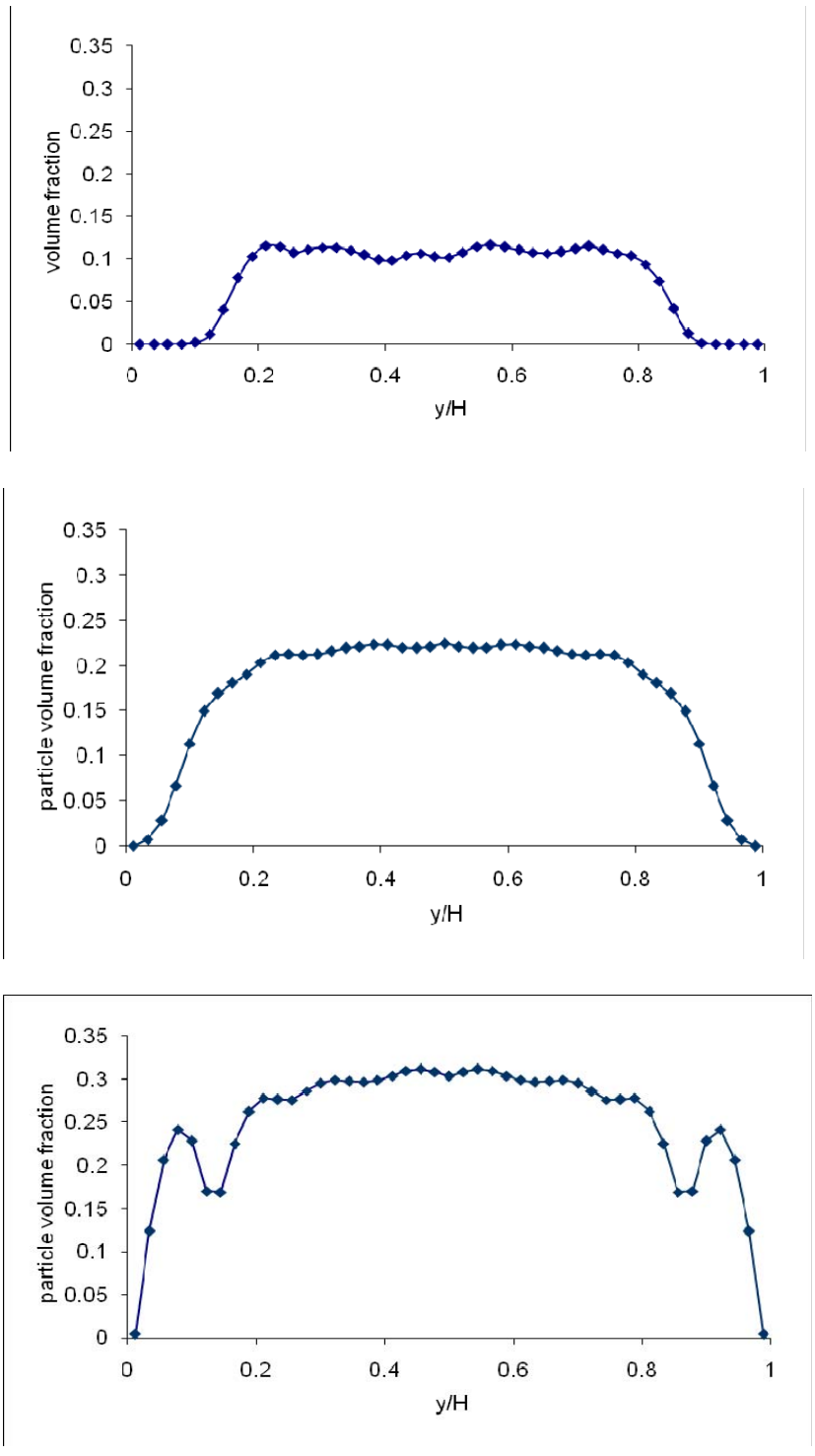


Figure 2.20 (a), (b), (c) Volume fraction distributions for Φ=0.1, 0.17 and 0.25 at H/a=15 and Re=0.5.

Table 2.2 The bulk volume fractions and depletion layer thickness for different Re, average volume fractions, and H/a.

| Re | <Φ> | H/a | $\Phi_b$ | Depletion layer thickness/a |
|---|---|---|---|---|
| 0.5 | 0.1 | 10 | 1.69E-01 | 2.05E+00 |
| | | 15 | 1.43E-01 | 2.25E+00 |
| | | 20 | 1.42E-01 | 2.94E+00 |
| | 0.17 | 10 | 2.45E-01 | 1.54E+00 |
| | | 15 | 2.25E-01 | 1.84E+00 |
| | | 20 | 2.20E-01 | 2.28E+00 |
| | 0.25 | 10 | 3.01E-01 | 8.48E-01 |
| | | 15 | 3.02E-01 | 1.30E+00 |
| | | 20 | 3.02E-01 | 1.73E+00 |
| 4 | 0.1 | 20 | 9.95E-02 | 5.0E-02 |
| | 0.17 | 20 | 1.75E-01 | 2.86E-01 |
| | 0.25 | 20 | 2.74E-01 | 8.76E-01 |

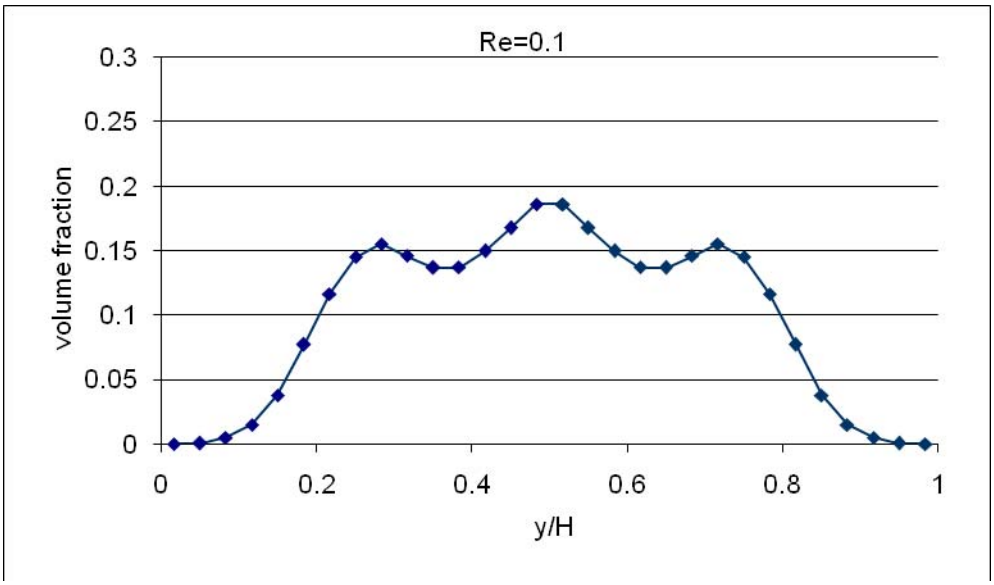


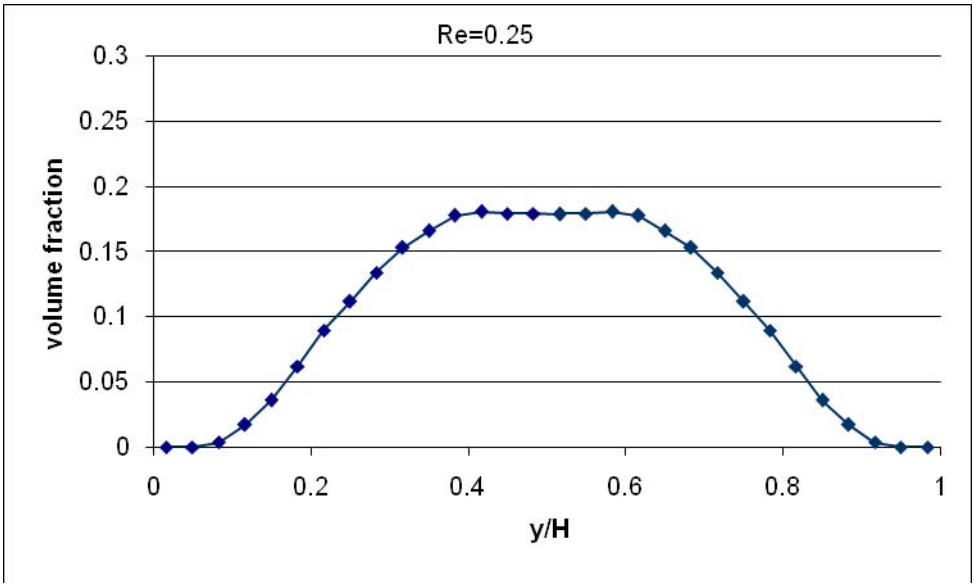


Figure 2.21 (a), (b) Volume fraction distribution for 0.1 at Re=0.1 and 0.25.

### 2.2.5 Inertial Migration of Particles

#### 2.2.5.1 Observation of Migration of Particles.

From Figure 2.21 (a, b), for Φ=0.1, there is a larger particle depletion region near the walls. This might due to particle migration. Due to the migration, there are more particles in the bulk region which generate larger $d_{BK}$ and fewer particles in the boundary layers which causes smaller $d_{BL}$.

#### 2.2.5.2 Introduction of inertial migration

The inertial migration of neutrally buoyant rigid spheres is first studied experimentally in poissueille flow by Segre & Silberberg (1962a, b). They found that in a dilute suspension, neutrally buoyant rigid particles attain an equilibrium position which is approximately 60% of the way from the centre-line to the walls. The migration of neutrally buoyant spherical particles in a Couette flow has been investigated experimentally by Halow (1968) and Halow & Wills (1970a, b). They find the spheres migrate to the centerline of the Couette cell.

Much research has attempted to obtain a theoretical description of the inertial migration phenomenon. Bretherton (1962) has shown that there is no lateral force if the inertia terms of the equations of motion are completely neglected. The migration is due to the inertia of the fluid. Most investigators have used asymptotic expansions for small values of the Reynolds number to estimate the inertial contribution to the lateral motion of the particle.

Cox & Brenner (1968) are the first to consider the Poiseuille flow by taking into account of the walls. They use the method of matched asymptotic expansions with two small parameters, the Reynolds number and the ratio of the sphere radius to the tube radius, to solve for the inertia-induced force and torque on the sphere. Ho & Leal (1974) obtain a similar result for a small sphere in a slow Poiseuille flow. This

migration velocity is proportional to the Reynolds number and wall velocity. The migration velocity predicted by Vasseur and Cox (1976) for a spherical particle suspended in a Couette flow is plotted in Figure 2.22. Feng and Joseph (1994) reported the results of a two-dimensional finite element simulation of the motion of a circular particle in a Couette flow. Their results are close to the Vasseur and Cox prediction when Re=0.625, but the difference is becoming larger when the inertial effect gets stronger. It is also noted that there could be a different result for circular particle and sphere. So the agreement could be fortuitous.

2.2.5.3 Inertial Migration Simulation and Drift Velocity

Single particle simulations were conducted to study inertial migration. Simulation conditions were: box size 30×30×30, particle radius 2.92, initial position at (3, 3, 3) for Re=0.25, 0.5 and at (8, 8, 8) for Re=0.1 because the migration velocity is too small near the wall. Migration velocity for different Reynolds numbers is compared with Vasseur & Cox theory (1976) (small Re requirement), shown in Figure 2.22. The result of Vasseur & Cox (1976) for an effectively bounded domain is also shown for comparison. There is a trend that when the Reynolds number is becoming smaller and smaller, the simulation results become closer to the Vasseur and Cox theoretical prediction. The migration near the wall is expected to be hindered by the presence of the wall when y/a is order one and this effect is no included in the theory. The theoretical prediction is for H/a>>1 and y/a>>1. So the results being lower than theory for small y are expected. The results for Re=0.1 and 0.25 are close together and this is expected if we are reaching the small Re asymptote.

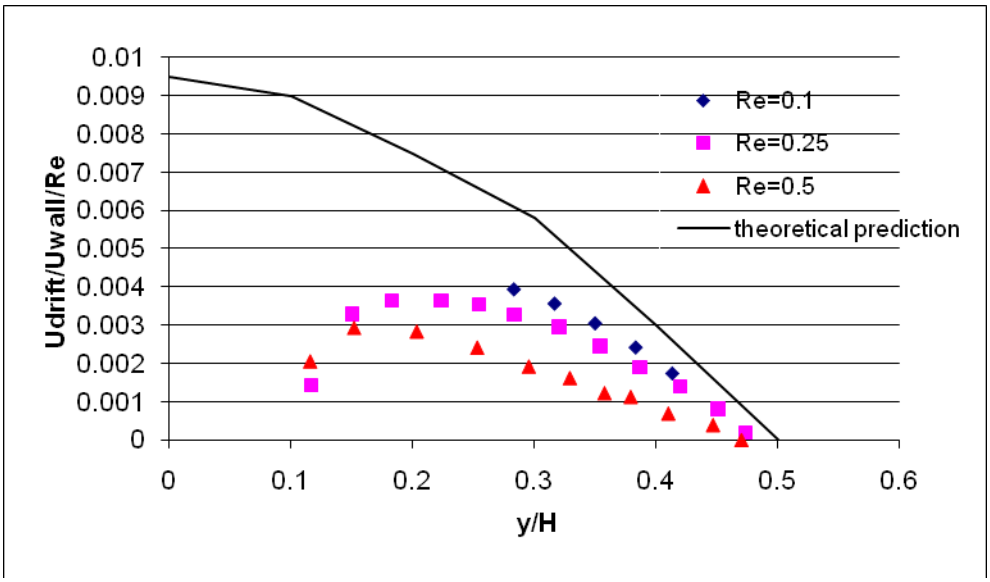


Figure 2.22 The migration velocity from the simulation and comparison with Vasseur and Cox theory. y/H=0 at the wall and y/H=0.5 in the center of the box.

2.2.5.4 Theoretical prediction for volume fraction distributions and comparison with simulations.

According to the conservation of solid particles, the volume fraction distribution of solid particles is calculated by using drift velocity from simulations, and compared with suspension simulation results.

$$\frac{d}{dy}(\,flux) = 0 \tag{2.2.1}$$

$$\frac{d}{dy}[V\Phi - D_P \frac{d\Phi}{dy}] = 0 \tag{2.2.2}$$

Where V –drift velocity of particle;

$D_P$ – diffusion coefficient of particle as function of $\dot{\gamma}$, a and Φ;

According to Leighton and Acrivos (1987),

$D_P = 0.5\dot{\gamma}a^2\Phi^2$ for low particle volume fraction

$$flux = 0 = V\Phi - D_P \frac{d\Phi}{dy} \tag{2.2.3}$$

$$V\Phi - 0.5\dot{\gamma}a^2\Phi^2 \frac{d\Phi}{dy} = 0 \tag{2.2.4}$$

$$\frac{d\Phi}{dy} = \frac{V}{0.5\dot{\gamma}a^2\Phi} \tag{2.2.5}$$

$$\int \Phi d\Phi = \int \frac{V(y)}{0.5\dot{\gamma}a^2} dy \tag{2.2.6}$$

As long as drift velocity is calculated from the simulation, the volume fraction distribution can be obtained according to equation (2.2.6). Predicted volume fractions for Re=0.1, 0.25 and 0.5 are shown in Figure 2.23(a), (b) and (c), compared to the suspension simulation results. The comparison of the predicted volume fractions with

the simulations results show the existence of the inertial migration of the particles. Due to the inertial migration, there are more particles in the bulk region which generate higher hydrodynamic diffusivity and there are fewer particles in the boundary layers which generates more boundary layer resistance. The combination of these two effects may have effect on the mass transfer.

## 2.3 Simulation Errors

### 2.3.1 Temporal Averaging

The mass transfer rate was typically found to reach a statistical steady state after a dimensionless time t^*_ss=$\dot{\gamma}$*t_ss (time to reach the steady state)=850. The Nusselt number was subsequently averaged over an additional time t^*_avr=850. The statistical uncertainty of the mass transfer rate estimated as the standard deviation of the Nusselt number obtained from five equal subintervals of the averaging time period was typically 3 to 7% of the mean value. For example, the Nusselt number for volume fraction 0.17 and H/a=10 was 2.33±0.15.

### 2.3.2 Time Step

The effect of time step on the mass transfer rate was studied at Re=1.5 and Pe=167. Nusselt numbers are 2.36±0.09 for dt=1 and 2.39±0.08 for dt=0.6. dt is in lattice units and the dimensionless times, defined as $\dot{\gamma}$ dt, are 1.76E-3 and 1.1E-3 respectively. The difference is negligible compared with the statistical error. Therefore, time step dt=1 is small enough to be used for the simulation.

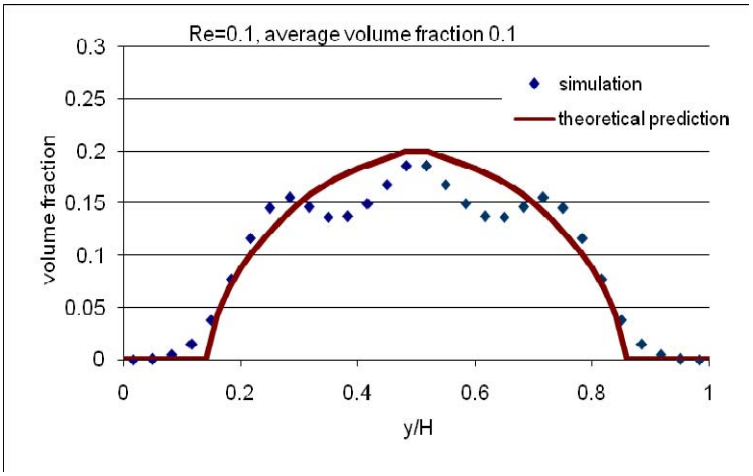


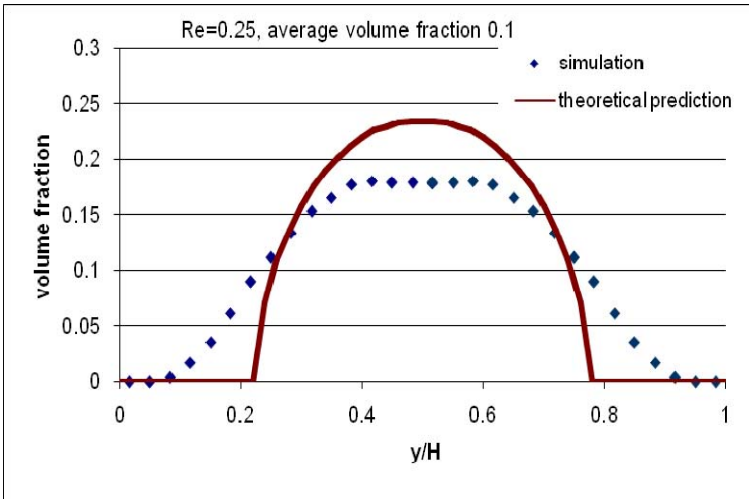


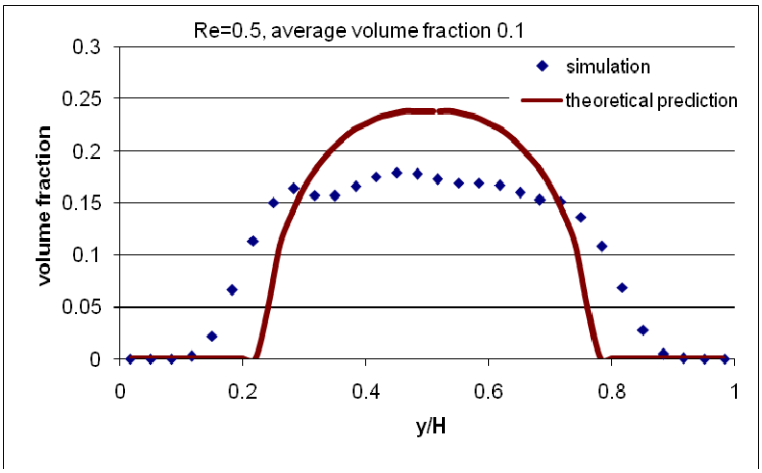


Figure 2.23 (a), (b) and (c) Predicted volume fraction compared with simulation results. (Re=0.1, 0.25 and 0.5).

### 2.3.3 Grid Resolution

The effect of grid resolution on the mass transfer rate was studied with boxsize of 60×60×60 with particle diameter 5.84 and with boxsize of 30×30×30 with particle diameter 2.92 at Pe=167, Re=0.5 and H/a=10. The Nusselt number for the first case is 2.59±0.18 and for the latter case is 2.33±0.15. Considering the statistical error of Nusselt number, the difference is negligible and grid resolution is enough for the boxsize of 30×30×30 with particle diameter 2.92.

### 2.3.4 Periodicity Length

Periodicity length has been chosen as 30 in x and z directions in all the previous simulations. The effect of periodicity length on the mass transfer was studied at Re=0.5 and Pe=167. The Nusselt number for boxsize of 30×30×30 which is in xyz directions, is 2.33±0.15 and the Nusselt number for boxsize of 45×30×45 is 2.41±0.18. The difference is small compared with the statistical error. Therefore, the periodicity length from 30 to 45 does not have any effect on the mass transfer rate.

## 3. Comparison of Experimental Results, Simulation Results with Theoretical Model

In addition to measuring and computing the overall rates of mass transport, it is desirable to understand the mechanisms that give rise to these results. The mass transfer across the Couette can be analyzed in terms of bulk and boundary layer resistances as was done for low Reynolds number and high Peclet number by Koch (1996). By understanding the separate effects of bulk and boundary layer resistances and the dependence of these resistances on Reynolds number, Peclet number, and solid particle volume fraction (Φ), a predictive model is developed for the mass transfer rate in sheared neutrally buoyant particle suspensions.

3.1 Theoretical model

Koch (1996) obtained a scaling analysis for the heat and mass transport in a sheared neutrally buoyant particle suspension. More details can be found in Chapter 1.

$$\frac{1}{Nu-1}=\frac{1}{d_2 Pe}+\frac{\pi a}{2^{1/2}H(d_3 Pe)^{1/4}} \qquad (2.3.1)$$

where $d_2$ and $d_3$ are the coefficients determined from experimental data.

In the Koch theory (1996), mass and heat transfer resistance includes two parts: bulk region and boundary layer. In the bulk region, mass transfer is proportional to Peclet number; in the boundary layers, mass transfer coefficient is proportional to $Pe^{1/4}$, as shown in equation 2.3.1. From the simulation results, these two resistances can be calculated separately. In the time-averaged concentration profile, as shown in Figure 2.18, in the bulk region the concentration gradient is a constant and can be calculated. There is a concentration slip near the walls. The definition of concentration slip is the concentration difference between the concentration at the wall and the concentration extrapolated from the bulk region, middle 1/3 of the region, by fitting straight line. The flux across the whole gap is Q and hydrodynamic diffusivity in the bulk region is $D_\infty$. So, in the bulk region,

$$Q=-D_\infty\left(\frac{dC}{dy}\right)_{bulk} \qquad (2.3.3)$$

$$\frac{D_\infty}{D}=d_2 Pe \qquad (2.3.4)$$

$d_2$ is constant and proportional to $\Phi^2$

In the boundary layer, $h_{BL}$ is mass transfer coefficient and $\Delta C$ is concentration slip.

$$h_{BL}\Delta C=Q \qquad (2.3.5)$$

Concentration slip and flux can both be calculated from simulations, and then $h_{BL}$ can be determined from equation 2.3.5. $d_2$ and $h_{BL}$ are shown in Figure 2.24 and Figure 2.25. $d_2$ and $h_{BL}$ are both constants. But according to the theory,

$$h_{BL} = \frac{2^{3/2}(d_3 Pe)^{1/4} D}{\pi a} \qquad (2.3.6)$$

$h_{BL}$ is proportional to $Pe^{1/4}$. The reason for this difference could be that Koch theory assumes Pe is large and then the concentration boundary layer thickness is much smaller than the radius of particle so that the fluctuating velocity is proportional to $y^2$ near the wall. But this scaling does not apply when Pe decreases. In the simulation with Pe up to 500, we calculate the boundary layer thickness corresponding to this $h_{BL}$ and find that it is comparable with the sphere radius. Although the scaling does not apply for smaller Peclet number, we still have a region on the order of particle radius where hydrodynamic diffusivity would be reduced. With assumption that the boundary layer thickness is a constant and on the order of particle radius, a modified theory is proposed.

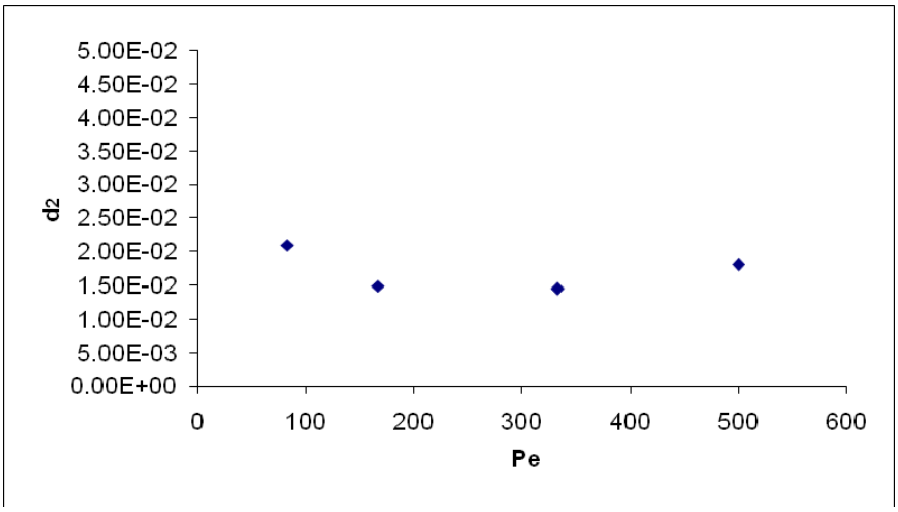


Figure 2.24 $d_2$ vs. Pe calculated from Koch theory (1996).

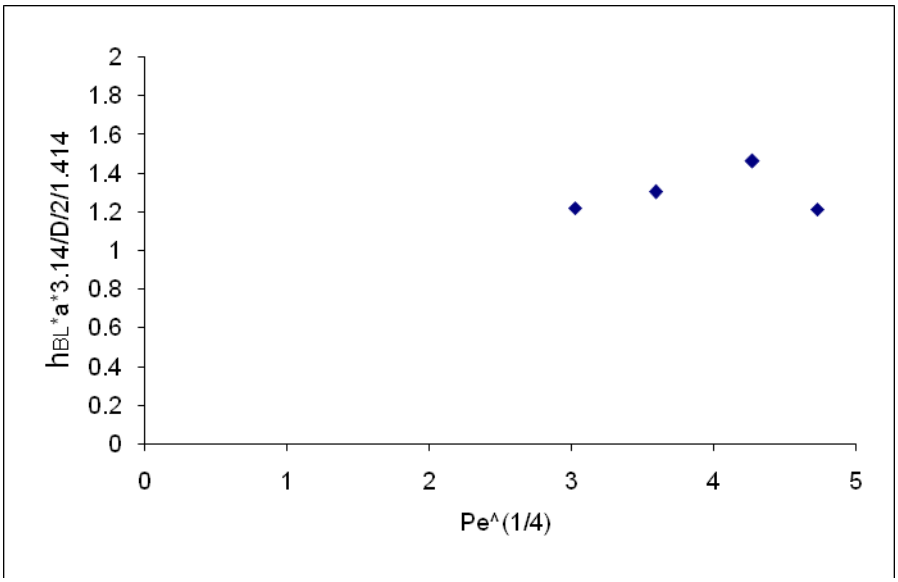


Figure 2.25 $h_{BL}$ vs. Pe calculated from Koch theory (1996).

3.2 Modified theory

The modified theory is illustrated in Figure 2.26. For small to medium Peclet numbers, the boundary layer thickness is assumed to be a constant δ independent of Pe, as shown in Figure 2.25. Within the boundary layer thickness, the Maxwell diffusivity ($D_M$) is playing an important role; in the bulk region (H-2δ), the effective diffusivity is the addition of hydrodynamic diffusivity ($D_H$) and Maxwell diffusivity. In the boundary layer and in the bulk region,

$$Flux = D_M \frac{C_\delta}{\delta} = \frac{1-2C_\delta}{H-2\delta}(D_H + D_M) = h \qquad (2.3.7)$$

From 2.3.7, $$C_\delta = \frac{1}{\frac{D_M^*(1-2\delta^*)}{\delta^*(D_H^* + D_M^*)} + 2} \qquad (2.3.8)$$

Where $D_M^*$ - Maxwell diffusivity non-dimensionlized by molecular diffusivity;

$\delta^*$ - the boundary layer thickness δ divided by gap thickness H;

h – the overall mass transfer coefficient.

By definition of Nusselt number and combined with equation (2.3.7),

$$Nu = \frac{hH}{D} = \frac{D_M{}^* C_\delta}{\delta^*} = \frac{1-2C_\delta}{1-2\delta^*}(D_H{}^* + D_M{}^*) \tag{2.3.9}$$

Combine equation (2.3.8) and (2.3.9),

$$\frac{1}{Nu} = \frac{1-2\delta^*}{D_H{}^* + D_M{}^*} + \frac{2\delta^*}{D_M{}^*}$$

$$\frac{1}{Nu} = \frac{1-2\delta/H}{d_{BK} Pe + D_M{}^*} + \frac{2\delta/H}{D_M{}^*} \tag{2.3.10}$$

Where $d_{BK}$ – coefficient in the bulk region, equivalent to $d_2$;

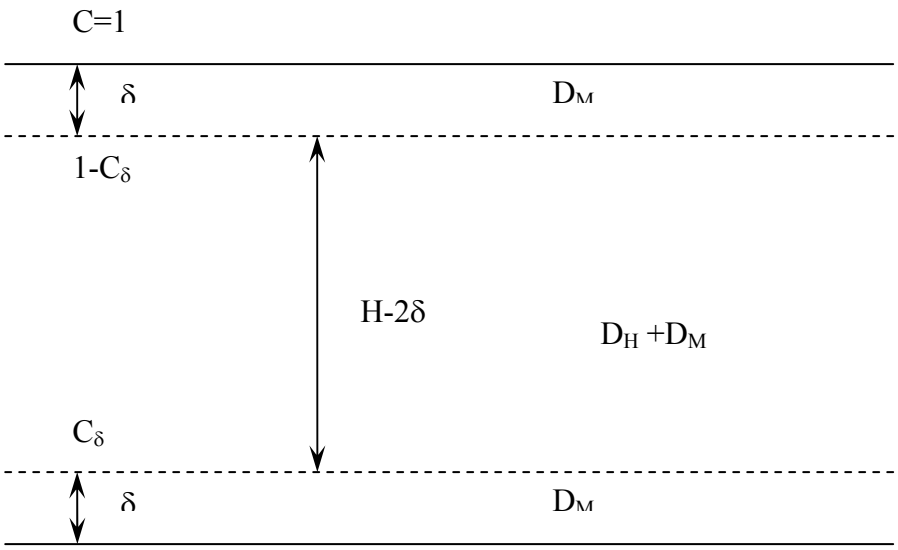


Figure 2.26 The illustration of the modified theory.

Assume $\delta=a/d_{BL}$ instead of $\delta=a/(d_3Pe)^{1/4}$ in Koch theory (1996), where $d_{BL}$ is a constant.

$$\frac{1}{Nu}=\frac{1-\frac{2a}{d_{BL}H}}{d_{BK}Pe+D_M^*}+\frac{\frac{2a}{d_{BL}H}}{D_M^*} \qquad (2.3.11)$$

From the concentration profile, the $d_{BK}$ and $d_{BL}$ can be determined. All $d_{BK}$ and $d_{BL}$ for different Re, volume fractions and H/a are listed in Table 2.3.

3.3 Summary of $d_{BK}$ and $d_{BL}$ for different H/a, volume fractions and Re

Table 2.3 $d_{BK}$ and $d_{BL}$ for different Re, volume fractions and H/a.

| Re | Volume fraction | H/a | $d_{BK}$ | $d_{BL}$ |
|---|---|---|---|---|
| 0.5 | 0.1 | 10 | 1.0E-02±3E-03 | 0.94±0.13 |
| | | 15 | 1.2E-02±2E-03 | 0.7±0.20 |
| | | 20 | 1.4E-02±5E-03 | 0.66±0.07 |
| | 0.17 | 10 | 1.7E-02±3E-03 | 1.52±0.14 |
| | | 15 | 1.6E-02±3E-03 | 1.35±0.13 |
| | | 20 | 1.7E-02±2E-03 | 1.2±0.08 |
| | 0.25 | 10 | 3.3E-02±7E-03 | 1.54±0.50 |
| | | 15 | 3.3E-02±2E-03 | 1.58±0.35 |
| | | 20 | 3.2E-02±4E-03 | 1.41±0.48 |
| 4 | 0.1 | 20 | 1.9E-02±2E-03 | 1.42±0.43 |
| | 0.17 | 20 | 2.5E-02±5E-03 | 1.85±0.66 |
| | 0.25 | 20 | 3.6E-02±5E-03 | 2.18±0.38 |

According to the modified theory, $d_{BK}$ and $d_{BL}$ are calculated for different volume fraction and H/a, as shown in Table 2.3. From the results, $d_{BK}$ is a constant, not changing with H/a for any given volume fraction. And $d_{BK}$ increases with volume fraction at any given H/a. This suggests that in the bulk region, H/a does not have any effect on hydrodynamic diffusion. According to Koch theory (1996), $d_{BK}$ is function of $\Phi^2$. Calculated $d_{BK}$ from simulation vs. $\Phi_b^2$ is shown in Figure 2.27 and compared with the prediction. The reason of $\Phi_b$ used here is because $d_{BK}$ is hydrodynamic diffusivity coefficient and is only a function of the volume fraction in the bulk. Due to the depletion region of particles near the wall, the volume fraction in the bulk is a little higher than the average volume fraction.

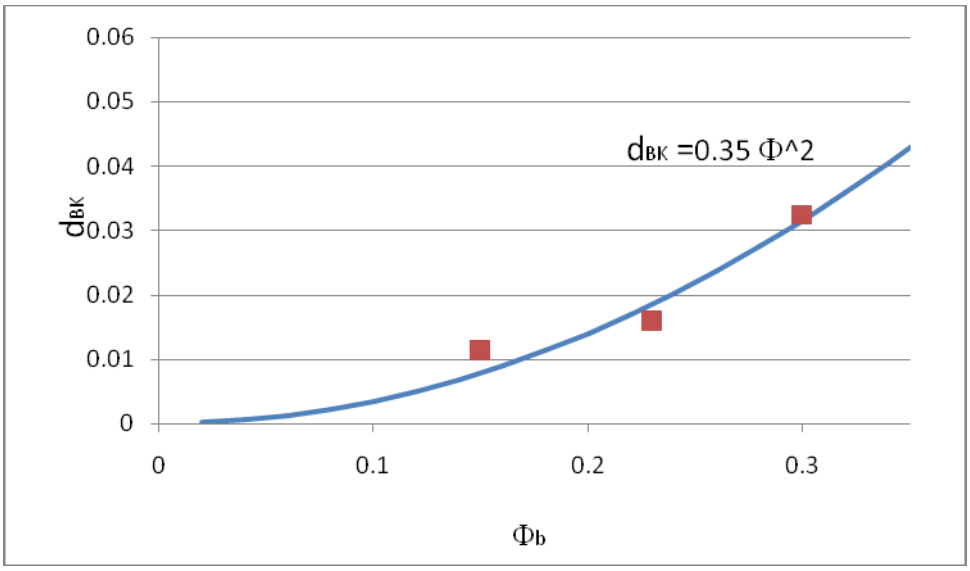


Figure 2.27 $d_{BK}$ from simulation vs. $\Phi_b^2$ and comparison with the theoretical prediction.

3.4 Simulation data compared with theory

According to the modified theory, $d_{BK}$ and $d_{BL}$ are calculated separately from the simulation results as showed before. Predicted Nu is compared to Nu obtained directly from the simulation in Figure 2.28, 2.29 and 2.30 for 17%, 25% and 10% respectively.

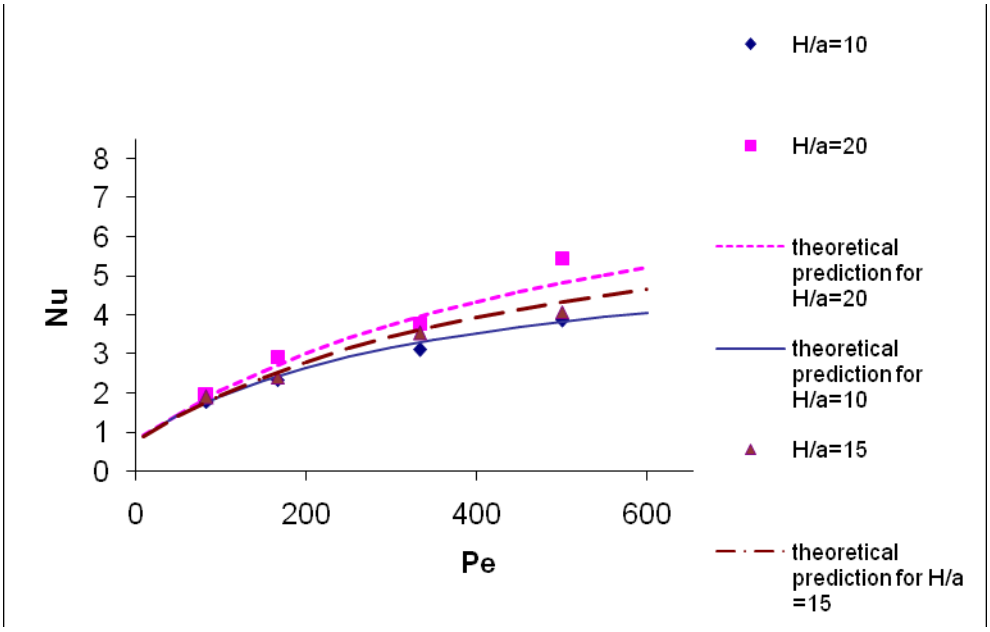


Figure 2.28 Simulated Nusselt number as function of Peclet number and H/a and comparison with the theoretical prediction for Φ=0.17 at Re=0.5.

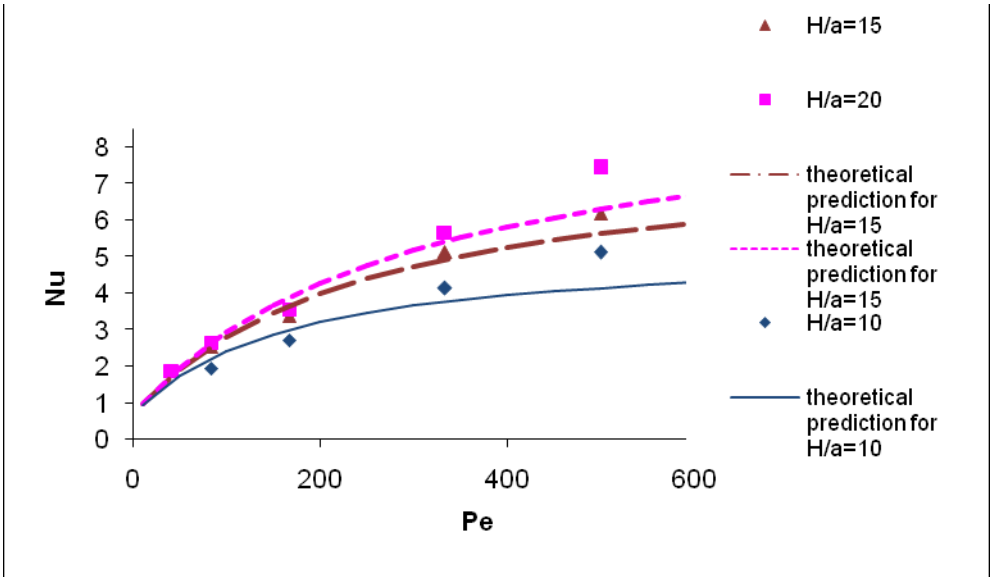


Figure 2.29 Simulated Nusselt number as function of Peclet number and H/a and comparison with the theoretical prediction for Φ=0.25 at Re=0.5.

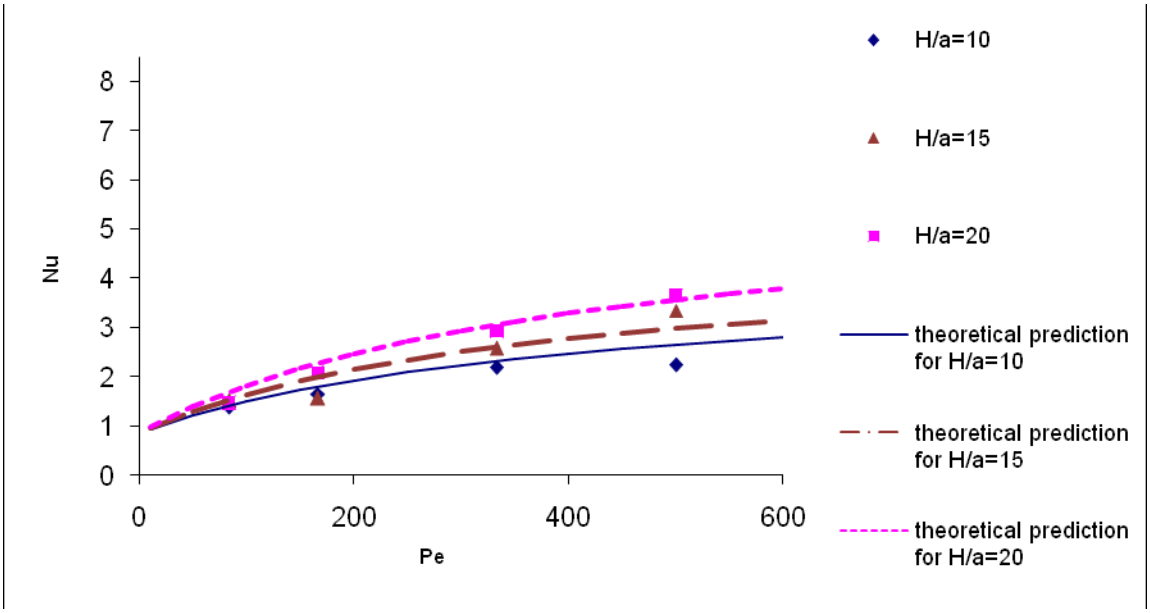


Figure 2.30 Simulated Nusselt number as function of Peclet number and H/a and comparison with the theoretical prediction for Φ=0.1 at Re=0.5.

3.5 Inertial effect

From Figure 2.17, inertia has an effect on the mass transfer rate. For $\Phi$=0.17 and H/a=10, Nu is a linear function of Reynolds number. According to equation (2.3.11), $d_{BK}$ and $d_{BL}$ are also assumed to be a linear function of Re. Simulations at Re=0.5 and Re=4 were conducted and $d_{BK}$ and $d_{BL}$ were calculated at these two different Reynolds numbers. Assume $d_{BK}$ and $d_{BL}$ are a linear function of Re, $d_{BK}$ and $d_{BL}$ dependence on Re are determined for different volume fractions.

3.6 Comparison of experimental data and theoretical prediction including Re effect.

Experiments were conducted with H/a =22 and H/a=44 at $\Phi$=0.1, 0.17 and 0.25. In order to compare with the theory, $d_{BK}$ and $d_{BL}$ have to be determined. Since $d_{BK}$ and $d_{BL}$ are function of H/a, the closest condition of simulations is H/a=20. So we use the values of $d_{BK}$ and $d_{BL}$ in the simulation of H/a=20. We also take into account of inertial effect because in the experiment, shear rate increase were used to increase the Peclet numbers. In the mean time, Re was also increased with shear rate. So $d_{BK}$ and $d_{BL}$ dependence on Re are used in the prediction. The dash lines are the prediction without taking into account of Re dependence. Without dependence on Re, Nu reaches asymptote value at high Pe. Obviously, predictions with $d_{BK}$ and $d_{BL}$ dependence on Re have good agreement with experimental results.

Similarly, $\Phi$=0.25 and 0.1 predictions are compared with experimental results, as shown in Figure 2.32 and Figure 2.33. For $\Phi$=0.17 and 0.25, theoretical predictions agree well with experimental results. For $\Phi$=0.1, predictions are larger compared with experimental results. This could be due to the statistical uncertainty of $d_{BK}$ and $d_{BL}$ shown in Table 2.3. The comparison with experimental data at high shear rates is particularly sensitive to the variation of $d_{BL}$ with Reynolds number. Therefore we plot in Figure 2.34, the comparison of the data with predictions based on the largest and

smallest estimates of the slope $d(d_{BL})/d(Re)$ obtained from the range of values of $d_{BL}$ at Re=0.5 and Re=4 reported in Table 2.3. Figure 2.34 shows that the experimental data is close to the prediction based on the smallest estimate of the slope. This observation indicates that the experimental measurements are consistent with the theory but that there is uncertainty in the comparison caused by the need to extrapolate the theory to higher values of Pe and Re than those explored in the simulations.

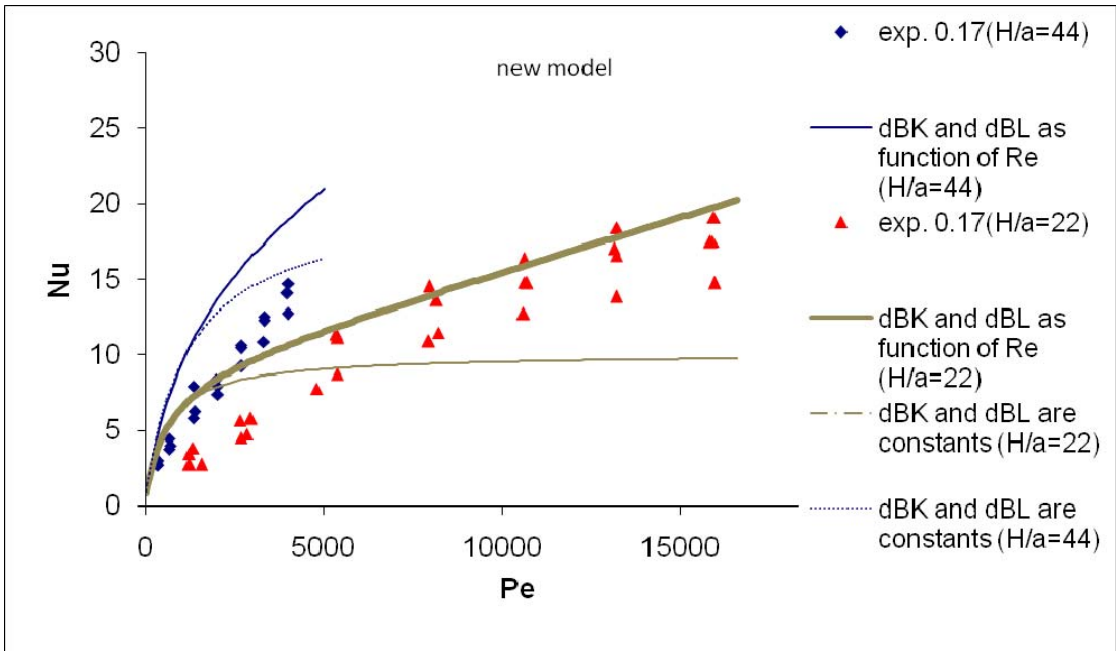


Figure 2.31 Comparison of experimental data and theoretical prediction with and without inertial effect for Φ=0.17.

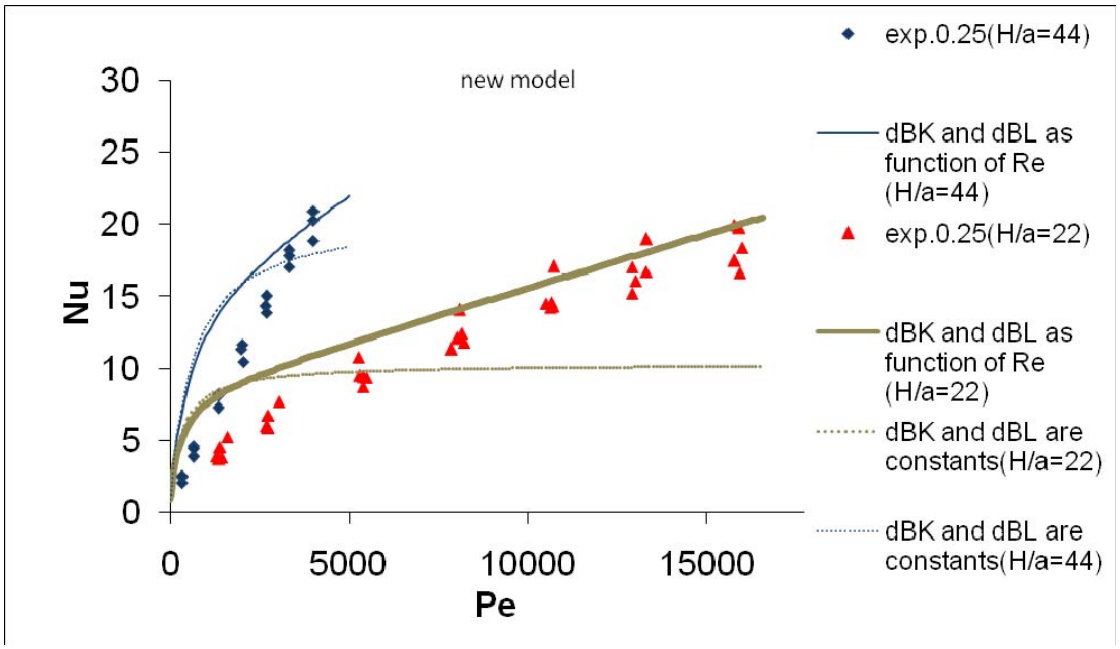


Figure 2.32 Comparison of experimental data and theoretical prediction with and without inertial effect for Φ=0.25.

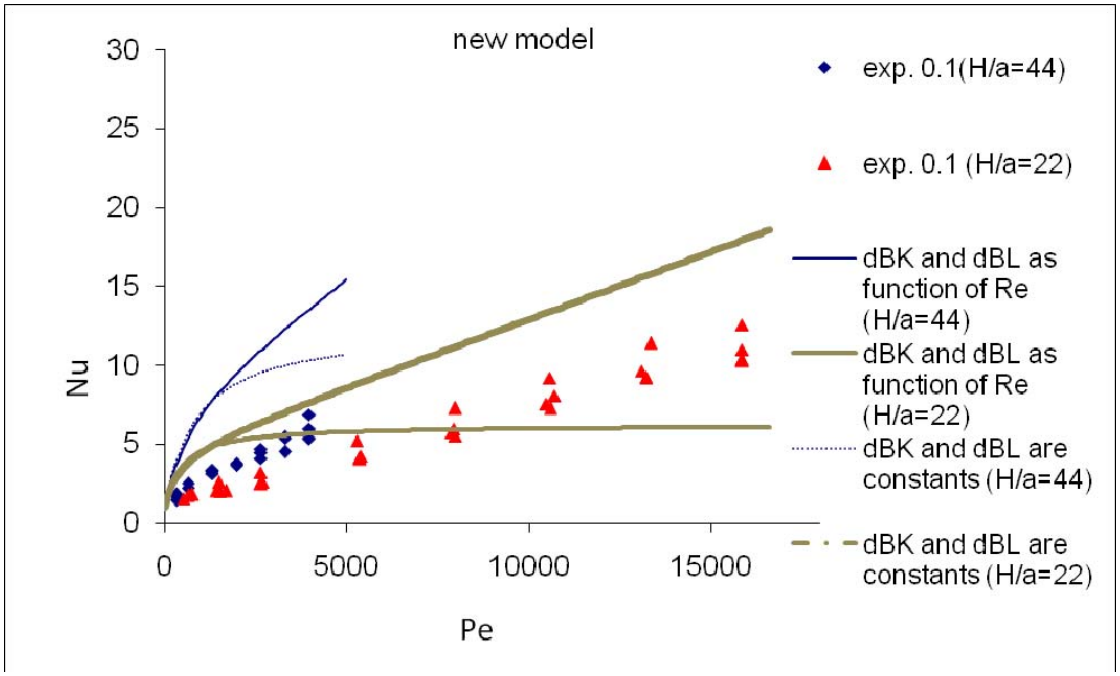


Figure 2.33 Comparison of experimental data and theoretical prediction with and without inertial effect for Φ=0.1.

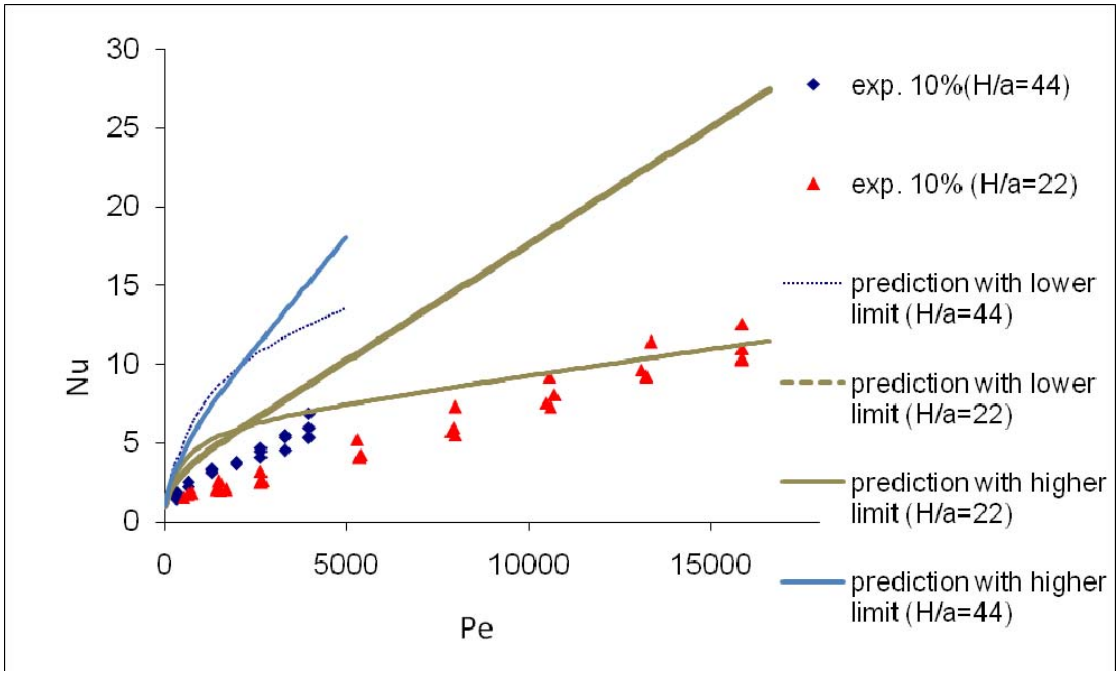


Figure 2.34 The theoreticla prediction with uncertainty range compared with experimental data at volume fraction 0.1.

## 4. Conclusions

Mass transfer was studied experimentally in Couette cell, with Re from 0 to 10, Pe from 0 to 15,870, H/a=22 and 44, volume fractions 0.1, 0.17, 0.25, 0.33 and 0.4. Experimental results show that mass transport rate increases with Peclet number.At lower Pe, Nu is almost linear function of Pe and at high Pe, Nu increases at a slower rate. Nu increases with volume fraction from 0.1 to 0.4. At higher volume fraction, increase rate becomes smaller.

Simulations were conducted for mass transport from $\Phi$=0.1, 0.17 and 0.25 at H/a=10, 15 and 20. Concentration profile shows that there is bulk region where concentration gradient is a constant and there are boundary layers near the walls where there is concentration slip. Mass transfer results show the same trends as in experiments: Nu increases with Pe, volume fraction and H/a. The inertial effect was studied. Migration effect was found at lower volume fraction (0.1) due to particle-wall interaction. Migration velocity was calculated and prediction of volume fraction distribution was made according to conservation of particles. This prediction agrees well with suspension simulations, which suggests the existence of migration.

A modified theory was proposed and constants were determined by simulations. $d_{BK}$ increases with volume fraction for different H/a and $d_{BL}$ decreases with H/a for different volume fractions. The prediction from this model agrees well with experimental data, suggesting that this model can be used to describe the heat and mass transfer in sheared neutrally buoyant particle suspensions.

# Chapter 3. Experimental Study of Mass Transfer from a Neutrally Buoyant Spherical Single Particle to Fluid in Simple Shear flow

## 3.1 Experiments

### 3.1.1 Principle of experiment (ion exchanger)

Ion exchange is a mass-transfer process. Ions are transferred from an aqueous solution to an ion-exchange polymerized resin, while an equivalent number of ions of the same charge, but of different species, are transferred in the opposite direction. The rate of exchange is governed by the same general considerations as for any mass-transfer in both phases, and the overall rate may be controlled by either or by both together of these resistances. Our concern is the mass transfer outside of the resin particles, so we chose to eliminate the diffusion process inside of the resin. Our experiments were carried out to approach this limiting case.

$Cl^-/OH^-$ ion exchanger of radius of 275μm was used in this study. Initially, ion exchanger was saturated by $OH^-$ and there was only $Cl^-$ in the solution. Due to the concentration gradient, $Cl^-$ diffused to the resin particle and exchanged with $OH^-$ and $OH^-$ diffused to the bulk solution.

$$ROH + KCl \rightarrow RCl + KOH$$

Where R is the resin particle.

Different ion solutions have different conductivities. Conductivity of the bulk solution as function of time characterized the mass transfer process.

The flux of ion exchange is

$$Flux = h(C_b - C_i) = -\frac{V}{A}\frac{dC_b}{dt} = -\frac{a}{3\Phi}\frac{dC_b}{dt}$$

Where h is the mass transfer coefficient;

A is the total exchange surface area of the resin particles;

$C_b$ is the $Cl^-$ concentration in the bulk;

$C_i$ is the $Cl^-$ concentration on the surface of the resin particles;

V is the total volume of the suspension;

a is the radius of resin particles;

Φ is the volume fraction of the resin particles;

In the initial period of ion exchange, $C_i \approx 0$,

Then, $h = -\frac{a}{3\Phi}\frac{d(\ln C_b)}{dt}$

$C_b$ as function of time was obtained from the conductivity of the solution measurement. Then the initial slop of this plot gave the value of $d(\ln C_b)/dt$ and Nu was determined. The Ln(C/C0) vs. time is shown in Figure 3.1, where C0 is the initial concentration of $Cl^-$ in the bulk solution.

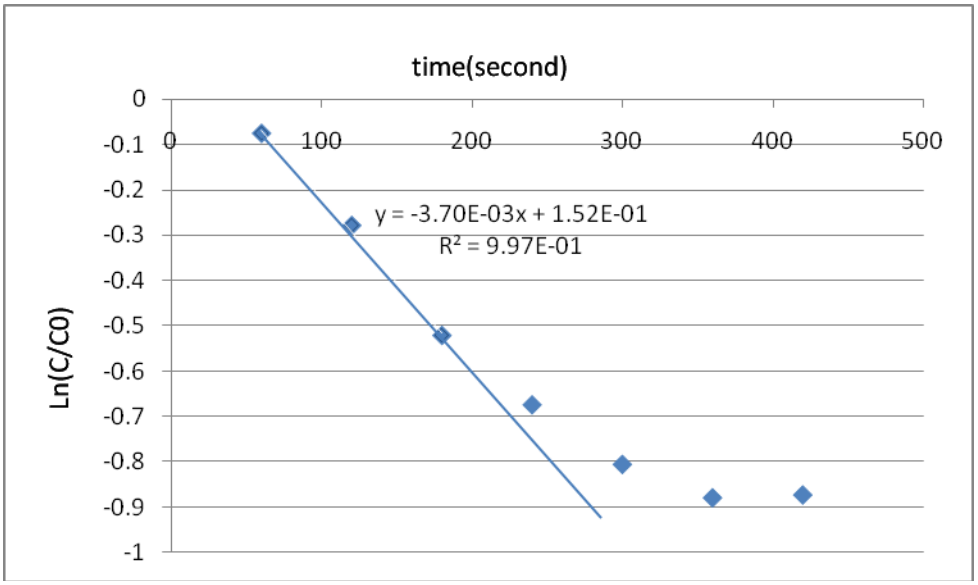


Figure 3.1 The $Cl^-$ concentration in the bulk solution vs. time and $d\ln(C_b)/dt$ obtained from the plot.

3.1.2 Experimental setup and procedures

A Couette Cell was used to attain the simple shear flow. This Couette cell included two concentric hollow cylinders and each cylinder consisted of three sections: the middle section was made of aluminum coated and top and bottom sections were made of transparent Plexiglas®. The transparent top and bottom parts could allow us to observe the suspensions inside of the Couette cell gap to assure the particles were uniformly suspended. The height of the metal parts was 12cm and of the Plexiglas® parts was 10cm. There were "O" rings which connected each Plexiglas® and metal parts. The inner diameter of the outer cylinder was 12cm and the gap thickness was 5mm, as shown in Figure 2.4. The inner cylinder was stationary and the outer cylinder could be rotated from 0 to 120 rpm. There was a Plexiglas® plate attached on the top of the inner cylinder to cover the gap between these two cylinders. There were one channel and six holes which were equally spaced in the angular direction in this plate, as shown in Figure 2.5. The high purity nitrogen was injected into this channel and then flowed out from the holes into the gap of the Couette cell and remained on the surface of the particle suspension, providing nitrogen blanket during the whole experimental process. The nitrogen protection can prevent the uptake of $CO_2$ from the air, which can dissolve in the solution and affect the conductivity measurement.

The $OH^-$ resin particles were used. The reason to choose $OH^-$ is because with the KCl in the bulk solution, it could minimize the effect of $CO_2$ uptaken from the air. The density of resin particles is $1.10 \times 10^3$ kg/m$^3$ at room temperature (22 °C). The glycery 60% (mass) – 0.014M KCl solution were used to match the density of the particles. The concentration of KCl was calculated based on the total volume of glycery/water solution. The resin particles were nearly neutrally buoyant in the solution. The radius of particle was 275 μm. The concentration of KCl was 0.014 M and glycerin was about 60% mass. The viscosity of the solution measured by capillary

viscometry was about $5.6\times10^{-3}$ pa·s. So kinematic viscosity of the solution $\nu=5.1\times10^{-6}$ $m^2/s$. According to Arvia (1967), the diffusivity is inversely proportional to the viscosity, so the averaged diffusivity of $Cl^-$ and $OH^-$ in the solution, $D=6.5\times10^{-10}$ $m^2/s$, was used in the calculation. The volume fraction of resin particle was ~0.023.

The glycery-KCl solution was prepared and mixed with resin particles. The suspension was transferred to the Couette Cell and samples were taken from the Couette cell at time minute 1, minute 2, … till minute 8. The sample was taken out by a syringe connected with a filter. So when the sample was taken out, the resin particles were separated with the solution, causing the ion exchange to stop. The conductivity of samples was measured by the conductivity meter (Accumet® AB30) and compared with the standard curve of concentration and conductivity. The standard curve was measured for known concentration of KCl and KOH. For example, the conductivities of 0.014M KCl, 0.007M KCl-0.007MKOH and 0.014M KOH were measured with 60% glycery. Then the concentration of KCl was plotted as function of conductivity. Since the concentration was low and concentration difference was small, the concentration was a linear function of conductivity. According to the standard curve, the concentration of $Cl^-$ as a function of time was plotted.

### 3.1.3 Conditions for experiment

The experiment was conducted under different rotation speed of outer cylinder from 4 rpm to 100 rpm which made the Reynolds number up to 1.5 and Peclet number up to 15,000.

## 3.2 Results and Discussion

### 3.2.1 Experimental results

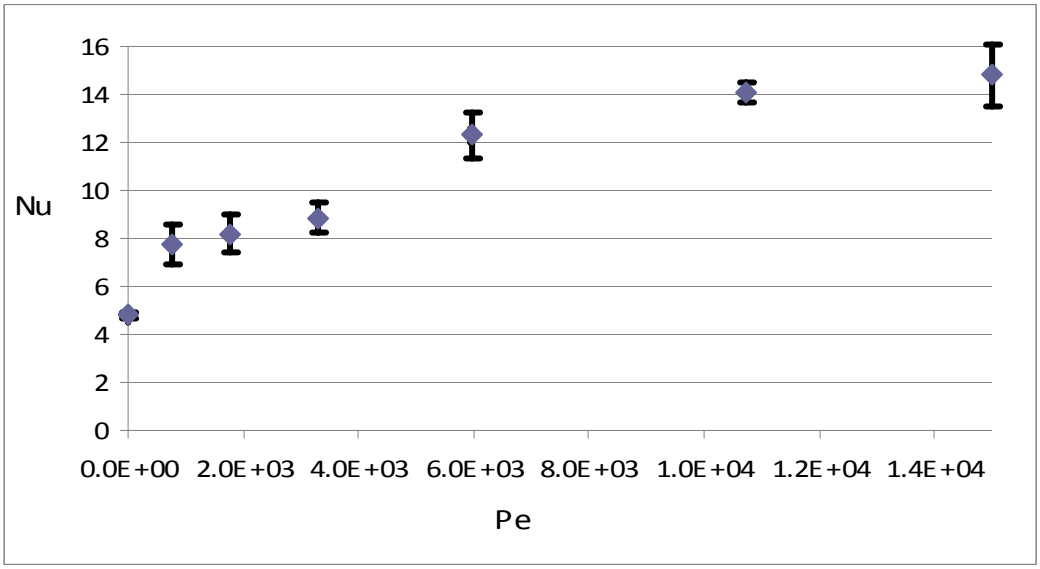


Figure 3.2 Nu as function of Peclet number. The standard deviations for each Pe are calcualted based on four independed runs of experiments.

### 3.2.2 Discussion of results

The results at 0rpm is consistently larger than 2 and it suggests that it is a systematic phenomenon. That could be due to nature convection.

Natural convection occurs when there is a density difference at the surface of the particles and in the bulk region. This effect can be characterized by Rayleigh number. The definition of Rayleigh number is

$$Ra = \frac{g\Delta\rho}{\rho}\frac{L^3}{\nu D}$$

Where g- gravitational acceleration;

$\Delta\rho$ - the density difference of KCl and KOH solutions;

L- πa for spherical particle;

a – the radius of particle;

ν- the kinematic viscosity;

D- the molecular diffusivity;

Churchill (1983) has developed a general correlation of convection with Ra,

$$Nu = (k_1 + 0.331 k_2 Ra^{1/6})^2$$

Where $k_1$=1.77 for spherical particle and

$k_2 = \frac{1.17}{[1+(0.5/Sc)^{9/16}]^{8/27}}$, where $Sc = \frac{\nu}{D}$.

For the experimental condition, $\Delta\rho=3.8\times10^{-3}$ kg/m$^3$, which is estimated from the CRC Handbook of Chemistry and Physics for 0.014M KCl and 0.014M KOH solutions, a=275μm, $\nu=5.1\times10^{-6}$ m$^2$/s, $D=6.5\times10^{-10}$ m$^2$/s, the corresponding Ra is 6.6 and Nu calculated from Churchill correlation is 5.28, which is comparable to the experimental result of 4.8 at 0rpm.

3.2.3 Comparison with simulations

Yang et al. (2007) numerically predict the Nusselt numbers for the mass transfer from a neutrally buoyant sphere in simple shear flow at finite $Pe$ and finite $Re$. They assume that the physical properties including mass diffusivity, fluid viscosity and density are constant and not influenced by the concentration of solute, no solid-liquid interface resistance to mass transfer exists and the concentration at the solid-liquid interface is constant. Thus, the mass transfer does not affect the flow structure and the solution of the simple shear flow and convective diffusion equations is decoupled. The momentum transfer problem can be solved first and the resulting velocity field is utilized to formulate the time evolution of mass transfer problem. The main calculation steps of this algorithm are outlined as follows: (1) initialize the flow field

(**u** and *P*) with the sphere at rest, physical parameters (density, viscosity and molecular diffusivity of solute), shear rate and concentration; (2) compute the velocity, pressure and rotation rate to steady state based on the torque-free rotation criterion using the SIMPLEC algorithm and Newton's method; (3) compute the unsteady concentration field in the fluid with the steady state flow field, and calculate the corresponding mass transfer Nusselt numbers.

As shown in Figure 3.3, the predicted Nu agrees with the experimental data. The experimental data are a little higher than the simulation results at higher Peclet numbers, which might be due to natural convection with higher centrifugal acceleration. The highest rotation speed was 120 rpm which corresponded to centrifugal acceleration of 9.46 $m/s^2$. The effective acceleration is 1.34 times of gravitational acceleration. Therefore, taken into consideration of centrifugal acceleration, the experimental data is comparable with the simulation results.

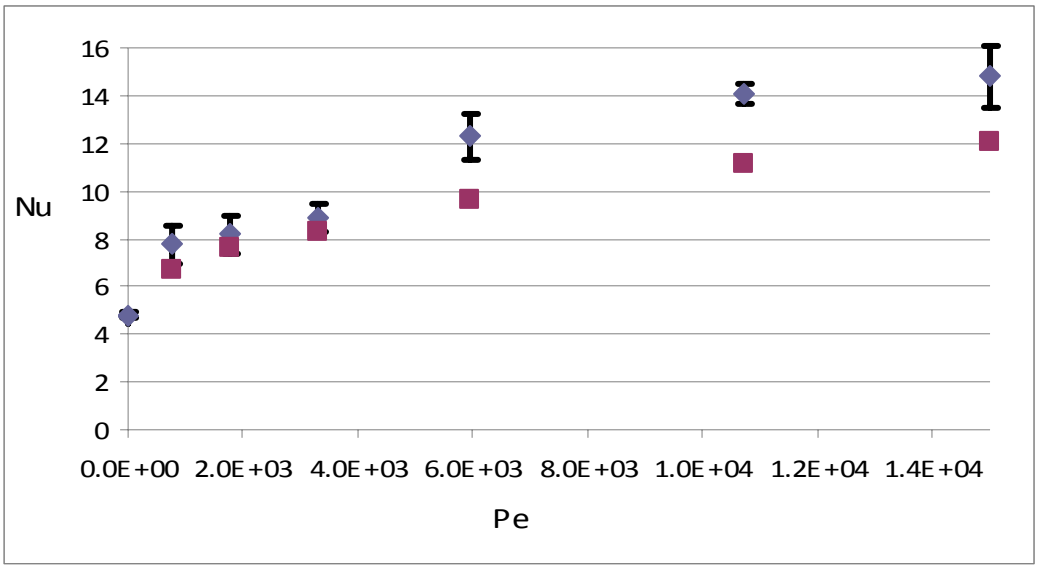


Figure 3.3. Comparison of experimental data with the simulation results (The diamonds with error bars are the experimental data and squares are the simulation results).

## 3.3 Conclusions

This chapter focuses on the experimental study of mass transfer from the neutrally buoyant particle to the bulk at finite Peclet number and Reynolds number. The Nusselt number is measured by ion exchange method. The Peclet number is up to 15,000 and Reynolds number is up to 1.5. The natural convection effect on the mass transfer is discussed. The experimental data agrees with the simulation results by Yang et al. (2007). The small discrepancy between the experimental data and simulation results may be due to the natural convection effect at higher centrifugal accelerations.

# REFERENCES

Acrivos, A. Heat transfer at high Peclet number from a small sphere freely rotating in a simple shear field. J. Fluid Mech., 1971, 46, 233

Armenante, P. M. and Kirwan, D. J. Mass transfer to microparticles in agitated systems. Chem. Eng. Sci., 1989, 44, 2701

Arvia, A. J., Marchiano,S.L. and Podesta, J. J. Diffusion of Ferrocyanide and Ferricyanide ions in aqueous solutions of potassium hydroxide. Electrochimica Acta 1967, 12 (3): 259

Asai, S., Konishi, Y. and Sasaki, Y. Mass transfer between fine particles and liquids in Agitated vessels. J. Chem. Eng. Jpn., 1988, 21, 107.

Bonnecaze, R.T., and Brady, J.F. The effective conductivity of random suspensions of spherical particles, Proc. R. Soc. Lond. A, 1991, 432, 445-465

Bretherton, F.P. The motion of rigid particles in a shear flow at low Reynolds number. J. Fluid Mech., 1962, 14, 284.

Calderbank, P. H. and Jones, S. R. J. Physical rate processes in industrial fermentation. Pat III. Mass transfer from fluids to solid particles suspended in mixing vessels. Trans. Inst. Chem. Eng. 1961, 39, 363

Cox, R.G. and Brenner, H. The lateral migration of solid particles in Poiseuille flow. Part 1. Theory. Chem. Engng Sci., 1968, 23, 147

Halow, J.S. 1968 Ph.D. thesis, Virginia Polytechnic Institute.

Halow, J.S. and Wills, G.B. Radial migration of spherical particles in Couette systems. AIChE J., 1970a, 16, 281.

Halow, J.S. and Wills, G.B. Experimental observations of sphere migration in Couette systems. Ind. Eng. Chem. Fund., 1970b, 9, 603

Harriott, P. Mass transfer to particles. Part I. Suspended in Agitated vessels. AIChe J. 1962, 8, 93

Ho, B.P. and Leal, L.G. Inertial migration of rigid spheres in two-dimensional unidirectional flows. J. Fluid Mech., 1974, 65, 365.

J. Feng, H.H.Hu and Joseph, D.D., Direct simulation of initial value problems for the motion of solid bodies in a Newtonian fluid. Part2. Couette and Poiseuille flows. J. Fluid Mech., 1994, 277: 271-301

Kuboi, R., Komasawa, I., Ohtake, T. and Iwasa, M. Fluid and particle motion in turbulent dispersion. Pat III. Paticle-liquid hydrodynamics and mass transfer in turbulent dispersion. Chem. Eng. Sci. 1974, 29, 659

Ladd, A.J.C. and Verberg, R. Lattice-Boltzmann simulations of particle-fluid suspensions. J. Stat. Phys.,2001, 104:1191-1251

Ladd, A.J.C. Numerical simulations of particulate suspensions via a discretized Boltzmann equation. Part 1. Theoretical foundation. J. Fluid Mech., 1994, 271:285-309

Ladd, A.J.C. Numerical simulations of particulate suspensions via a discretized Boltzmann equation. Part 2. Numerical results. J. Fluid Mech., 1994, 271:311-339

Ladd, A.J.C. and Verberg, R. Lattice-Boltzmann simulations of particle-fluid suspensions. Journal of Statistical Physics, 2001, 104, 1191-1251

Leal, L.G., On the Effective Conductivity of a Dilute Suspension of Spherical Drops in the Limit of Low Particle Peclet Number, Chemical Engineering communications, Vol. 1, 1973, pp. 21-31.

Leighton, D. and Acrivos, A., Measurement of shear-induced self-diffusion in concentrated suspensions of spheres, J. Fluid Mech., 1987, 177: 109-131

Maxwell, J.C., Electricity and magnetism, vol. 1, Clarendon, Oxford, 1892

Nir, N., and Acrivos, A., "The Effective Thermal Conductivity of Sheared Suspensions," Journal of Fluid Mechanics, 1976, 78, 33-48.

Robertson, C. R. and Acrivos, A. Low Reynolds number shear flow past a rotating circular cylinder 1. Momentum transfer J. Fluid Mech., 1970, 40, 685

Robertson, C. R. and Acrivos, A. Low Reynolds number shear flow past a rotating circular cylinder. 2. Heat transfer. J. Fluid Mech., 1970, 40, 705

Rubinow, R.V. and Keller, J.B. The transverse force on a spinning sphere moving in a viscous fluid. J. Fluid Mech., 1961, 11, 447.

Saffman, P.G. The lift on a small sphere in a slow shear flow. J. Fluid Mech., 1965, 22, 385

Sangani, A.S. and Acrivos, A. Slow flow through a periodic array of spheres. Int. J. Multiphase Flow, 1982, 8:343-360

Schlichting, H. Boundary layer theory, McGraw-Hill, New York, 1955, P. 357

Segre, G., Silberberg, A. Behavior of macroscopic rigid spheres in Poiseuille flow. Part1. J. Fluid Mech., 1962a, 14, 115.

Segre, G., Silberberg, A. Behavior of macroscopic rigid spheres in Poiseuille flow. Part 2. J. Fluid Mech., 1962b, 14, 136.

Selman, J.R. and Tobias, C.W. Mass-transfer measurements by the limiting-current technique, Adv. Chem. Eng. 1978, 10, 211-318

Sohn, C.W. and Chen, M.M. Microconvective thermal conductivity in disperse two-phase mixtures as observed in a low velocity Couette flow experiment. J. Heat Transfer, 1981, 103, 47.

Subramanian, G. and Koch, D. L. Centrifugal forces alter streamline topology and greatly enhance the rate of heat and mass transfer from neutrally buoyant particles to a shear flow Phys. Rev. Lett., 2006, 96, 134503

Subramanian, G. and Koch, D. L. Inertial effects on the transfer of heat or mass from neutrally buoyant spheres in a steady linear velocity field. Phys. Fluids, 2006, 18, 073302

Turner, J.C.R. Two phase conductivity: The electrical conductance of liquid-fluidized beds of spheres. Chem. Engng Sci., 1976, 31, 487.

Vasseur, P. and Cox, R.G. The lateral migration of a spherical particle in two-dimensional shear flows. J. Fluid Mech., 1976, 78, 385.

Verberg, R. and Koch, L. Rhology of particle suspensions with low to moderate fluid inertia at finite particle inertia. Physics of fluids,2006, 18, 083303

Wang, N.-H. L. and Keller, K.H. Augmented transport of extracellular solutes in concentrated erythrocyte suspensions in Couette flow. J. Colloid Interface Sci., 1985, 103, 210

Wang, N.L. Thesis 1978 Effects of Fluid Shear on the Mass Transport Properties of Erythrocyte Suspensions

Yagi, H., Motouchi, T. and Hikita, H. Mass Transfer from fine particles in a stirred vessel: effect of surface area of particle. Ind. Eng. Chem. Process Des. Dev. 1984, 23, 145

Yang, C., Wang, L. and Koch, D. L., (Writing) Effect of inertial on the mass/heat transfer from a neutrally buoyant sphere at finite Reynolds number in simple shear flow.

Yin, X.L. Thesis, Structure-property relations in bubble and solid particle suspensions with moderate Reynolds numbers, 2007

Zydney, A. L. and Colton, C. K. Augmented solute transport in the shear flow of a concentrated suspension. Physico-Chem. Hydrodyn, 1988, 16, 77